

# On the stability of dust orbits in mean motion resonances with considered perturbation from an interstellar wind

P. Pástor

*Tekov Observatory, Sokolovská 21, 934 01 Levice, Slovak Republic*

pavol.pastor@hvezdarenlevice.sk, pastor.pavol@gmail.com

## ABSTRACT

Circumstellar dust particles can be captured in a mean motion resonance with a planet and simultaneously be affected by non-gravitational effects. It is possible to describe secular variations of a particle orbit in the mean motion resonance analytically using averaged resonant equations. We derived the averaged resonant equations from the equations of motion in near-canonical form. The secular variations of the particle orbit depending on the orientation of the orbit in space are taken into account. The averaged resonant equations can be derived/confirmed also from Lagrange's planetary equations. We applied the derived theory to the case when the non-gravitational effects are the Poynting–Robertson effect, the radial stellar wind, and an interstellar wind. The analytical and numerical results obtained are in excellent agreement. We found that the types of orbits correspond to libration centers of the conservative problem. The averaged resonant equations can lead to a system of equations which hold for stable orbits during the synodic period. Using this system we show analytically that for the considered non-gravitational effects, there does not exist any stable orbit with an advance of pericenter. Numerical solutions of this system show that none stable orbits with a fixed pericenter for both the exact and non-exact resonance exist.

*Subject headings:* Interplanetary dust, Mean motion resonances, Averaged resonant equations, Poynting–Robertson effect, Stellar wind, Interstellar matter

## 1. Introduction

A small body orbiting a star with a planet is affected by the planet's gravitational field. When the orbital periods of the body and the planet have a ratio of small natural numbers, mean motion resonances (MMRs) can occur. If the body is captured in an MMR, then variations of the semimajor axis are balanced by the resonant interaction with the planet's field of gravity. Examples of MMRs in the Solar system are numerous. We can mention MMRs of asteroids with Jupiter which have resulted in the formation of the Kirkwood gaps in the main asteroid belt (Kirkwood 1867), MMRs of particles in Saturn's rings with its moons, MMRs of the Edgeworth–Kuiper belt objects with

Neptune, MMRs of dust particles with the Earth (Brownlee 1994; Dermott et al. 1994; Reach et al. 1995), and so on. Following the observational confirmation of dust particles being captured in MMRs with the Earth by satellites *IRAS* (Dermott et al. 1994) and *COBE* (Reach et al. 1995), unknown properties of orbital evolution for dust particles captured in MMRs have become an interesting topic of research.

If the planet moves in a circular orbit around the star and the mass of the particle is negligible in comparison with the mass of the star and also in comparison with the mass of the planet, we have a special gravitational problem of three bodies. This gravitational problem is called the circular restricted three-body problem (CR3BP) in celestial mechanics.

Unlike larger bodies such as the planets or moons, dust particles can be significantly affected by weak non-gravitational forces. The acceleration of the particle caused by electromagnetic radiation described by the Poynting–Robertson (PR) effect (Poynting 1904; Robertson 1937; Klačka et al. 2014) was used within the framework of the planar CR3BP by Beaugé & Ferraz-Mello (1994) in order to obtain stationary solutions for dust particles captured in MMRs. They found that for all dust particles captured in a given exterior resonance (the orbital period of the particle in the exterior resonance is larger than the planet’s orbital period), the eccentricities of the orbits approach a constant value, which they called the “universal eccentricity”. Their derivation starts from a near-canonical form of the equations of motion in Cartesian coordinates with the PR effect used as a dissipative external acceleration (for dissipative accelerations in the CR3BP and periodic orbits see also Margheri, Ortega & Rebelo 2012). Another near-canonical approach was used in Gomes (1995) in order to determine which non-gravitational forces (with assumed behavior leading to the universal eccentricity) give a stable, and which an unstable, capture in an exterior resonance within the framework of the planar CR3BP. The author began from a near-canonical system of equations written in Delaunay variables. The secular time derivative of the eccentricity for a dust particle captured in an MMR in the planar CR3BP under the action of arbitrary non-gravitational effects can be obtained using the method presented in Gomes (1995). Within the framework of the CR3BP, there exists a constant, referred to as the Jacobi constant, which depends on the position and velocity of the particle and the position of the planet. Under the assumptions that the particle is far enough from the planet and that the mass of the planet is negligible compared to the mass of the star, the Jacobi constant reduces to the so called Tisserand parameter. The Tisserand parameter depends only on the Keplerian orbital elements of the particle and the planet. For the PR effect, the universal eccentricity was confirmed using a different derivation starting from the secular time derivative of the Tisserand parameter by Liou & Zook (1997). In Liou & Zook (1997), also, a general relation between the secular time derivatives of the eccentricity and inclination during the orbital evolution of a dust particle captured in an MMR in the CR3BP with the PR effect and a radial stellar wind (for the wind, see Gustafson 1994; Klačka et al. 2012) has been found. In Gomes (1997) are derived the secular time derivatives of the eccentricity and inclination from both a Jacobi constant approach and another approach explicitly using the disturbing function. The equations are deduced depending on in which kind of resonance there is a trapping. The influence

of the PR effect and a non-radial stellar wind (Klačka et al. 2012) on the secular evolution of the eccentricity for a dust particle captured in an MMR within the framework of the planar CR3BP was analytically investigated in Klačka et al. (2008) and Pástor et al. (2009). The secular evolutions of the eccentricity and the argument of pericenter of a dust particle captured in an MMR in the planar circular and elliptical restricted three-body problem with the PR effect were numerically investigated in Pástor, Klačka & Kómar (2009).

The influence of an interstellar wind on the motion of dust particles was already mentioned in Whipple (1955). Observations of debris disks around stars show that the interaction of the interstellar wind with the dust particles of the disk can change the shape of the debris disks (Hines et al. 2007; Maness et al. 2009; Debes, Weinberger & Kuchner 2009; Buenzli et al. 2010; Rodigas et al. 2012). From among only 16 debris disks resolved in scattered light (Golimowski et al. 2011) as many as three disks show a changed morphology caused by the interaction with the surrounding interstellar matter. The acceleration acting on a spherical body moving through an interstellar gas was published in Baines, Williams & Asebiomo (1965). This acceleration was used in the calculation of the secular time derivatives of the Keplerian orbital elements caused by an interstellar gas flow (IGF) for an arbitrary orientation of the orbit in Pástor, Klačka & Kómar (2011) and Pástor (2012b). The secular decrease of the semimajor axis for all initial conditions was found. This result was confirmed analytically by Belyaev & Rafikov (2010) and numerically by Marzari & Thébault (2011) and Marzari (2012). Belyaev & Rafikov (2010) used an orbit-averaged Hamiltonian approach to determine the orbital evolution of a dust particle in a Keplerian potential subject to an additional constant force. If the speed of the IGF is much greater than the speed of the dust grain and also much greater than the mean thermal speed of the gas in the flow, then the acceleration caused by the IGF reduces to a constant vector. Therefore, the problem which they solved can be applied to the orbital motion of a dust particle under the action of an IGF. The secular orbital motion in this case can be completely solved analytically (Pástor 2012a).

In Pástor (2013), the results of Pástor (2012b) were used in order to obtain the secular time derivative of the orbit eccentricity for a dust particle captured in an MMR within the framework of the planar CR3BP with the PR effect, a radial stellar wind, and an IGF. The agreement between the analytical and numerical results in Pástor (2013) was excellent for the IGF in the Solar system. The results show that two sets of orbital evolutions divided by a strong boundary in the initial conditions exist for the exterior 2/1 resonance. Also, some kind of stabilization was found in one of these sets. These results motivated us to determine some basic properties of the orbital evolution of a dust particle captured in an MMR in the planar CR3BP with the PR effect, a radial stellar wind, and an IGF, using the improved methods from Beaugé & Ferraz-Mello (1993).

## 2. Averaged resonant equations

We will consider the motion of a homogeneous spherical dust particle in the vicinity of a star with one planet moving in a circular orbit (CR3BP). Non-gravitational effects will be added to the

CR3BP framework. The secular variations of the particle orbit caused by these non-gravitational effects can depend on the orientation of the orbit in space. Taking into account this dependence, we will improve the method presented in Beaugé & Ferraz-Mello (1993) for the study of problems which involve non-gravitational effects without a spherical symmetry around the star.

The equation of motion can be written in the form

$$\frac{d\vec{v}}{dt} = \frac{\partial F}{\partial \vec{r}} + \vec{Y} , \quad (1)$$

where  $\vec{v} = d\vec{r}/dt$  is the velocity of the dust particle,  $\vec{r}$  is the position vector of the dust particle with respect to the star,  $F$  is the Hamiltonian of the conservative system, and  $\vec{Y}$  is the non-conservative part of the acceleration. If we add to Eq. (1) equations for the velocity in the Cartesian coordinates, we obtain a system of equations in the near-canonical form:

$$\frac{d\vec{r}}{dt} = \frac{\partial F}{\partial \vec{v}} , \quad \frac{d\vec{v}}{dt} = \frac{\partial F}{\partial \vec{r}} + \vec{Y} . \quad (2)$$

Following Beaugé & Ferraz-Mello (1993), we will use canonical variables derived from the Delaunay variables in the extended phase space. The canonical variables are  $l_j = (\lambda, \tilde{\omega}, t)$  and  $L_j = (L, G-L, \Lambda)$ , where  $\lambda$  is the mean longitude,  $\tilde{\omega}$  is the longitude of pericenter,  $L = \sqrt{\mu(1-\beta)}a$ ,  $G = L\sqrt{1-e^2}$ , and  $\Lambda$  is the canonical momentum that is conjugate to time. In the canonical variables  $\mu = G_0M_\star$ ,  $G_0$  is the gravitational constant,  $M_\star$  is the mass of the star,  $a$  is the semimajor axis of the particle orbit, and  $e$  is the eccentricity of the particle orbit. From the non-gravitational effects, the electromagnetic radiation of the star in the form of the Poynting–Robertson (PR) effect is most often considered. The parameter  $\beta$  is defined as the ratio between the electromagnetic radiation pressure force and the gravitational force between the star and the particle at rest with respect to the star

$$\beta = \frac{3L_\star \bar{Q}'_{\text{pr}}}{16\pi c \mu R \rho} . \quad (3)$$

Here,  $L_\star$  is the stellar luminosity,  $\bar{Q}'_{\text{pr}}$  is the dimensionless efficiency factor for the radiation pressure averaged over the stellar spectrum and calculated for the radial direction ( $\bar{Q}'_{\text{pr}} = 1$  for a perfectly absorbing sphere), and  $R$  is the radius of the dust particle with mass density  $\rho$ . The radial term not depending on the particle velocity in the PR effect (Eq. 21) can be added to the stellar gravity because its net effect is only to reduce the mass of the star to  $M_\star(1-\beta)$ . Therefore, we use  $L = \sqrt{\mu(1-\beta)}a$ . Using the Brouwer–Hori theorem (Brouwer & Hori 1961), we can transform Eqs. (2) into a new system of near-canonical equations

$$\frac{dl_j}{dt} = -\frac{\partial F}{\partial L_j} + Q_j , \quad \frac{dL_j}{dt} = \frac{\partial F}{\partial l_j} + P_j , \quad (4)$$

where

$$Q_j = \sum_{k=1}^3 Y_k \frac{\partial r_k}{\partial L_j} , \quad P_j = \sum_{k=1}^3 Y_k \frac{\partial r_k}{\partial l_j} \quad (5)$$

and  $r_k$  are the Cartesian coordinates of the particle position vector with respect to the star. A cumbersome calculation of the partial derivatives finally yields

$$\begin{aligned}
 Q_1 &= \frac{2}{L} \vec{Y} \cdot \vec{r} + (1 - \alpha) Q_2 , \\
 Q_2 &= \frac{a}{Le} \vec{Y} \begin{pmatrix} \alpha \cos \tilde{\omega} - e \sin E \sin \tilde{\omega} \\ \alpha \sin \tilde{\omega} + e \sin E \cos \tilde{\omega} \end{pmatrix} - \frac{\alpha}{Le} P_1 \sin E , \\
 P_1 &= \frac{1}{n} \vec{Y} \cdot \vec{v} , \\
 P_2 &= \vec{Y} \begin{pmatrix} -r_2 \\ r_1 \end{pmatrix} - P_1 ,
 \end{aligned} \tag{6}$$

where  $\alpha = \sqrt{1 - e^2}$ ,  $E$  is the eccentric anomaly, and  $n = \sqrt{\mu(1 - \beta)/a^3}$  is the mean motion of the particle. Eqs. (6) differ from the equations in Beaugé & Ferraz-Mello (1993) due to the dependence of the partial derivatives on the orientation of the orbit of the particle in space, which is taken into consideration. The Hamiltonian of the conservative system in the new variables is

$$F = \frac{\mu^2(1 - \beta)^2}{2L^2} - \Lambda + R , \tag{7}$$

where  $R$  is the disturbing function

$$R = G_0 M_P \left( \frac{1}{|\vec{r} - \vec{r}_P|} - \frac{\vec{r} \cdot \vec{r}_P}{r_P^3} \right) , \tag{8}$$

$M_P$  is the mass of the planet, and  $\vec{r}_P$  is the position vector of the planet with respect to the star and  $r_P = |\vec{r}_P|$ . The subscript P will be used for quantities belonging to the planet. In order to investigate the behavior of a particle captured in an MMR with a planet in a circular orbit, we will use the canonical resonant variables  $H, K, \sigma_1, J_1, \sigma_2, J_2$

$$\begin{aligned}
 H &= \sqrt{2|L - G|} \sin(\psi/q - \tilde{\omega}) , & K &= \sqrt{2|L - G|} \cos(\psi/q - \tilde{\omega}) , \\
 \sigma_1 &= \psi/q - \tilde{\omega}_P , & J_1 &= G + \Lambda/n_P , \\
 \sigma_2 &= (\lambda - \lambda_P)/q , & J_2 &= (p + q)L + p\Lambda/n_P ,
 \end{aligned} \tag{9}$$

where  $p$  and  $q$  are two integers and  $\psi = (p + q)\lambda_P - p\lambda$ . A second application of the Brouwer–Hori theorem yields equations which are formally consistent with the set of equations presented in

Beaugé & Ferraz-Mello (1993):

$$\begin{aligned}
 \frac{dH}{dt} &= -\frac{\partial F}{\partial K} - \frac{H}{H^2 + K^2} P_2 + K(sQ_1 + Q_2) , \\
 \frac{dK}{dt} &= \frac{\partial F}{\partial H} - \frac{K}{H^2 + K^2} P_2 - H(sQ_1 + Q_2) , \\
 \frac{d\sigma_1}{dt} &= -\frac{\partial F}{\partial J_1} + sQ_1 , \\
 \frac{dJ_1}{dt} &= \frac{\partial F}{\partial \sigma_1} + P_1 + P_2 , \\
 \frac{d\sigma_2}{dt} &= -\frac{\partial F}{\partial J_2} - \frac{1}{q} Q_1 , \\
 \frac{dJ_2}{dt} &= \frac{\partial F}{\partial \sigma_2} + (p + q)P_1 ,
 \end{aligned} \tag{10}$$

where  $s = p/q$ . All terms in the disturbing function depending on  $\tilde{\omega}_P$  contain powers of  $e_1$  as factors due to the d'Alembert property (Murray & Dermott 1999). Because we are considering only circular planetary orbits, and  $\tilde{\omega}_P$  is only present in  $\sigma_1$ , we have  $\partial F/\partial \sigma_1 = 0$ . Eqs. (10) have to be averaged over a synodic period. The change of  $\sigma_2$  is equal to  $2\pi$  during the synodic period. The term  $\partial F/\partial \sigma_2$  in Eqs. (10), when averaged over the synodic period, becomes  $1/2\pi \int_0^{2\pi} \partial F/\partial \sigma_2 d\sigma_2 = F(2\pi) - F(0) = 0$  due to the periodicity of the disturbing function with this period (during the averaging). Thus, Eqs. (10) averaged over the synodic period become

$$\begin{aligned}
 \frac{dH}{dt} &= -\frac{\partial F}{\partial K} - \frac{H}{H^2 + K^2} \langle P_2 \rangle + K(s \langle Q_1 \rangle + \langle Q_2 \rangle) , \\
 \frac{dK}{dt} &= \frac{\partial F}{\partial H} - \frac{K}{H^2 + K^2} \langle P_2 \rangle - H(s \langle Q_1 \rangle + \langle Q_2 \rangle) , \\
 \frac{d\sigma_1}{dt} &= -\frac{\partial F}{\partial J_1} + s \langle Q_1 \rangle , \\
 \frac{dJ_1}{dt} &= \langle P_1 \rangle + \langle P_2 \rangle , \\
 \frac{d\sigma_2}{dt} &= -\frac{\partial F}{\partial J_2} - \frac{1}{q} \langle Q_1 \rangle , \\
 \frac{dJ_2}{dt} &= (p + q) \langle P_1 \rangle .
 \end{aligned} \tag{11}$$

In resonant problems, it is convenient to study the behavior in the non-canonical variables  $(k, h) = (e \cos \sigma_0, e \sin \sigma_0)$ , where  $\sigma_0 = \psi/q - \tilde{\omega}$ .  $J_1$  can be expressed using  $L$ ,  $J_2$ ,  $k$ , and  $h$  in the disturbing function  $R$ . The number of equations can be reduced from six to five because  $dJ_2/dt$  can be expressed using  $dL/dt$  and  $dJ_1/dt$ . The equation for  $dJ_1/dt$  can be replaced by an equation for  $dL/dt$ . A further reduction in the number of equations is possible because  $\sigma_2$  is cyclic and can

be ignored. Therefore, only four equations remain:

$$\begin{aligned}
\frac{dk}{dt} &= \frac{\alpha}{L} \frac{\partial R}{\partial h} - h \frac{d\sigma_1}{dt} - \frac{k\alpha}{L(1+\alpha)} \frac{dL}{dt} - \frac{k\alpha}{Le^2} \langle P_2 \rangle - h \langle Q_2 \rangle , \\
\frac{dh}{dt} &= -\frac{\alpha}{L} \frac{\partial R}{\partial k} + k \frac{d\sigma_1}{dt} - \frac{h\alpha}{L(1+\alpha)} \frac{dL}{dt} - \frac{h\alpha}{Le^2} \langle P_2 \rangle + k \langle Q_2 \rangle , \\
\frac{dL}{dt} &= s \left( h \frac{\partial R}{\partial k} - k \frac{\partial R}{\partial h} \right) + \langle P_1 \rangle , \\
\frac{d\sigma_1}{dt} &= n_P \frac{p+q}{q} - ns + \frac{2sL}{\mu(1-\beta)} \frac{\partial R}{\partial a} - \frac{\alpha s}{L(1+\alpha)} \left( k \frac{\partial R}{\partial k} + h \frac{\partial R}{\partial h} \right) + s \langle Q_1 \rangle . \tag{12}
\end{aligned}$$

Eqs. (12) represent averaged resonant equations that include the directional character of the non-conservative acceleration  $\vec{Y}$ . It is worth mentioning that the averaged values of the non-conservative terms  $\langle Q_j \rangle$  and  $\langle P_j \rangle$  can be expressed using the averaged values of  $da/dt$ ,  $de/dt$ ,  $d\tilde{\omega}/dt$ , and  $d\sigma_b/dt + t dn/dt$  caused by the non-gravitational effects only. The angle  $\sigma_b$  is defined so that the mean anomaly can be computed from  $M = nt + \sigma_b$  (Bate, Mueller & White 1971). On the left-hand sides of Eqs. (12), we can use Lagrange's planetary equations in the form

$$\begin{aligned}
\frac{da}{dt} &= \frac{2}{na} \frac{\partial R}{\partial \sigma_b} + \left\langle \frac{da}{dt} \right\rangle_{\text{EF}} , \\
\frac{de}{dt} &= \frac{\alpha^2}{na^2e} \frac{\partial R}{\partial \sigma_b} - \frac{\alpha}{na^2e} \frac{\partial R}{\partial \tilde{\omega}} + \left\langle \frac{de}{dt} \right\rangle_{\text{EF}} , \\
\frac{d\sigma_b}{dt} + t \frac{dn}{dt} &= -\frac{2}{na} \frac{\partial R}{\partial a} - \frac{\alpha^2}{na^2e} \frac{\partial R}{\partial e} + \left\langle \frac{d\sigma_b}{dt} + t \frac{dn}{dt} \right\rangle_{\text{EF}} , \\
\frac{d\tilde{\omega}}{dt} &= \frac{\alpha}{na^2e} \frac{\partial R}{\partial e} + \left\langle \frac{d\tilde{\omega}}{dt} \right\rangle_{\text{EF}} . \tag{13}
\end{aligned}$$

$\partial R/\partial a$  in Eqs. (13) is calculated in such a way that  $n$  is treated as a constant (Danby 1988). For this particular case this is the only correct way and this also cancels the term  $\langle t dn/dt \rangle_G$  (where the subscript G denotes that the change is caused by gravitation only) in the derivation resulting from  $d\sigma_1/dt$  in Eqs. (12). During these operations the following relations have to be used:

$$\begin{aligned}
\frac{\partial R}{\partial \sigma_b} &= -s \frac{\partial R}{\partial \sigma_0} , \\
\frac{\partial R}{\partial \tilde{\omega}} &= -\frac{p+q}{q} \frac{\partial R}{\partial \sigma_0} , \\
\frac{\partial R}{\partial \sigma_0} &= k \frac{\partial R}{\partial h} - h \frac{\partial R}{\partial k} , \\
e \frac{\partial R}{\partial e} &= k \frac{\partial R}{\partial k} + h \frac{\partial R}{\partial h} . \tag{14}
\end{aligned}$$

The relations obtained are

$$\begin{aligned}
\langle Q_1 \rangle &= - \left\langle \frac{d\tilde{\omega}}{dt} \right\rangle_{\text{EF}} - \left\langle \frac{d\sigma_b}{dt} + t \frac{dn}{dt} \right\rangle_{\text{EF}} , \\
\langle Q_2 \rangle &= - \left\langle \frac{d\tilde{\omega}}{dt} \right\rangle_{\text{EF}} , \\
\langle P_1 \rangle &= \frac{na}{2} \left\langle \frac{da}{dt} \right\rangle_{\text{EF}} , \\
\langle P_2 \rangle &= - \frac{na(1-\alpha)}{2} \left\langle \frac{da}{dt} \right\rangle_{\text{EF}} - \frac{na^2e}{\alpha} \left\langle \frac{de}{dt} \right\rangle_{\text{EF}} .
\end{aligned} \tag{15}$$

Eqs. (15) hold for arbitrary non-gravitational effects.

### 3. The secular time derivative of the eccentricity of the orbit

The second equation of Eqs. (13) yields

$$\begin{aligned}
\frac{de}{dt} &= \frac{\alpha^2}{na^2e} \frac{\partial R}{\partial \sigma_b} - \frac{\alpha}{na^2e} \frac{\partial R}{\partial \tilde{\omega}} + \left\langle \frac{de}{dt} \right\rangle_{\text{EF}} \\
&= \frac{\alpha^2}{2ae} \left( \frac{da}{dt} - \left\langle \frac{da}{dt} \right\rangle_{\text{EF}} \right) + \frac{\alpha}{na^2e} \frac{p+q}{q} \frac{\partial R}{\partial \sigma_0} + \left\langle \frac{de}{dt} \right\rangle_{\text{EF}} ,
\end{aligned} \tag{16}$$

where also the first equation of Eqs. (13) and the second equation of Eqs. (14) were used. If we use the first equation of Eqs. (14) and the first equation of Eqs. (13) in Eq. (16), then we obtain

$$\begin{aligned}
\frac{de}{dt} &= \frac{\alpha^2}{2ae} \left( \frac{da}{dt} - \left\langle \frac{da}{dt} \right\rangle_{\text{EF}} \right) - \frac{\alpha}{2ae} \frac{p+q}{p} \left( \frac{da}{dt} - \left\langle \frac{da}{dt} \right\rangle_{\text{EF}} \right) + \left\langle \frac{de}{dt} \right\rangle_{\text{EF}} \\
&= \frac{\alpha}{2ae} \left( \alpha - \frac{p+q}{p} \right) \frac{da}{dt} + \frac{\alpha}{2ae} \left( \frac{p+q}{p} - \alpha \right) \left\langle \frac{da}{dt} \right\rangle_{\text{EF}} + \left\langle \frac{de}{dt} \right\rangle_{\text{EF}} .
\end{aligned} \tag{17}$$

This equation can be averaged over a resonant libration period of the semimajor axis and the result is

$$\left\langle \frac{de}{dt} \right\rangle = \frac{\alpha}{2ae} \left( \frac{p+q}{p} - \alpha \right) \left\langle \frac{da}{dt} \right\rangle_{\text{EF}} + \left\langle \frac{de}{dt} \right\rangle_{\text{EF}} , \tag{18}$$

because

$$\left\langle \frac{da}{dt} \right\rangle = 0 . \tag{19}$$

Eq. (18) is consistent with the same result obtained from an averaging of the time derivative of the Tisserand parameter over the resonant libration period of the semimajor axis (see Gomes 1997; Pástor, Klačka & Kómar 2009; Pástor 2013) and with the same result obtained from a near-canonical approach Gomes (1995, 1997). We can rewrite Eq. (18) using the averaged non-conservative terms in Eqs. (15)

$$\left\langle \frac{de}{dt} \right\rangle = \frac{\alpha}{na^2e} \left( \frac{1}{s} \langle P_1 \rangle - \langle P_2 \rangle \right) . \tag{20}$$



#### 4. The effects that will be considered

We take into account the electromagnetic radiation of the star, the radial stellar wind, and the interstellar gas flow (IGF).

##### 4.1. Electromagnetic radiation

The acceleration of the homogeneous spherical dust particle caused by the electromagnetic radiation of the star is given by the PR effect (Poynting 1904; Robertson 1937; Klačka et al. 2014). The acceleration to first order in  $v/c$  ( $v$  is the speed of the dust particle with respect to the star and  $c$  is the speed of light in vacuum) has the form

$$\frac{d\vec{v}}{dt} = \beta \frac{\mu}{r^2} \left[ \left( 1 - \frac{\vec{v} \cdot \vec{e}_R}{c} \right) \vec{e}_R - \frac{\vec{v}}{c} \right], \quad (21)$$

where  $r = |\vec{r}|$  is the distance from the star and  $\vec{e}_R = \vec{r}/r$  is the radial unit vector.

##### 4.2. Radial stellar wind

The acceleration caused by the radial stellar wind is, to first order in  $v/c$  and first order in  $v/u$  ( $u$  is the speed of the stellar wind with respect to the star) (Klačka et al. 2012, Eq. 37):

$$\frac{d\vec{v}}{dt} = \frac{\eta}{Q'_{\text{pr}}} \beta \frac{u}{c} \frac{\mu}{r^2} \left[ \left( 1 - \frac{\vec{v} \cdot \vec{e}_R}{u} \right) \vec{e}_R - \frac{\vec{v}}{u} \right]. \quad (22)$$

Here,  $\eta$  is the ratio of the stellar wind energy to the electromagnetic stellar energy, both radiated per unit time

$$\eta = \frac{4\pi r^2 u}{L_\star} \sum_{i=1}^N n_{\text{sw } i} m_{\text{sw } i} c^2, \quad (23)$$

where  $m_{\text{sw } i}$  and  $n_{\text{sw } i}$ ,  $i = 1$  to  $N$ , are the masses and concentrations of the stellar wind particles at a distance  $r$  from the star ( $u = 450$  km/s and  $\eta = 0.38$  for the Sun, Klačka et al. 2012).

##### 4.3. Interstellar gas flow

The acceleration caused by the flow of neutral gas can be given in the form (Baines, Williams & Asebiomo 1965)

$$\frac{d\vec{v}}{dt} = - \sum_i c_{\text{Di}} \gamma_i |\vec{v} - \vec{v}_F| (\vec{v} - \vec{v}_F). \quad (24)$$

The sum in Eq. (24) runs over all particle species  $i$ .  $\vec{v}_F$  is the velocity of the IGF in the frame associated with the star,  $c_{\text{Di}}$  is the drag coefficient, and  $\gamma_i$  is the collision parameter. The drag

coefficient can be calculated from

$$c_{\text{Di}}(s_i) = \frac{1}{\sqrt{\pi}} \left( \frac{1}{s_i} + \frac{1}{2s_i^3} \right) e^{-s_i^2} + \left( 1 + \frac{1}{s_i^2} - \frac{1}{4s_i^4} \right) \text{erf}(s_i) + (1 - \delta_i) \left( \frac{T_{\text{d}}}{T_i} \right)^{1/2} \frac{\sqrt{\pi}}{3s_i}, \quad (25)$$

where  $\text{erf}(s_i)$  is the error function  $\text{erf}(s_i) = 2/\sqrt{\pi} \int_0^{s_i} e^{-t^2} dt$ ,  $\delta_i$  is the fraction of impinging particles specularly reflected at the surface (for the resting particles, there is assumed diffuse reflection) (Baines, Williams & Asebiomo 1965; Gustafson 1994),  $T_{\text{d}}$  is the temperature of the dust grain, and  $T_i$  is the temperature of the  $i$ th gas component.  $s_i$  is defined as a molecular speed ratio

$$s_i = \sqrt{\frac{m_i}{2kT_i}} U. \quad (26)$$

Here,  $m_i$  is the mass of the neutral atom in the  $i$ th gas component,  $k$  is Boltzmann's constant, and  $U = |\vec{v} - \vec{v}_{\text{F}}|$  is the relative speed of the dust particle with respect to the gas. For the collision parameter, we can write

$$\gamma_i = n_i \frac{m_i}{m} A, \quad (27)$$

where  $n_i$  is the concentration of the  $i$ th kind of interstellar neutral atom,  $A = \pi R^2$  is the geometric cross section of the spherical dust grain, and  $m$  is the grain mass. Using the approximation that the speed of the IGF is much greater than the speed of the dust grain in the frame associated with the star ( $|\vec{v}| = v \ll |\vec{v}_{\text{F}}| = v_{\text{F}}$ ), an approximate expression for the relative speed is

$$U = |\vec{v} - \vec{v}_{\text{F}}| = \sqrt{v^2 + v_{\text{F}}^2 - 2\vec{v} \cdot \vec{v}_{\text{F}}} \approx v_{\text{F}} \left( 1 - \frac{\vec{v} \cdot \vec{v}_{\text{F}}}{v_{\text{F}}^2} \right). \quad (28)$$

The same approximation can be used also in Eq. (25). The result is

$$\begin{aligned} c_{\text{Di}}(s_i) &\approx c_{\text{Di}}(s_{0i}) + \left( \frac{dc_{\text{Di}}}{ds_i} \right)_{s_i=s_{0i}} (s_i - s_{0i}) \\ &\equiv c_{\text{Di}}(s_{0i}) + \left( \frac{dc_{\text{Di}}}{ds_i} \right)_{s_i=s_{0i}} \sqrt{\frac{m_i}{2kT_i}} (U - v_{\text{F}}) \\ &\approx c_{0i} - k_i \frac{\vec{v} \cdot \vec{v}_{\text{F}}}{v_{\text{F}}}, \end{aligned} \quad (29)$$

where

$$\begin{aligned} s_{0i} &\equiv \sqrt{\frac{m_i}{2kT_i}} v_{\text{F}}, \\ c_{0i} &\equiv c_{\text{Di}}(s_{0i}), \\ k_i &\equiv \left( \frac{dc_{\text{Di}}}{ds_i} \right)_{s_i=s_{0i}} \sqrt{\frac{m_i}{2kT_i}}. \end{aligned} \quad (30)$$

Rewriting Eq. (24) using Eqs. (28) and (29) yields

$$\frac{d\vec{v}}{dt} = - \sum_i c_{0i} \gamma_i v_F^2 \left[ \frac{\vec{v}}{v_F} - \frac{\vec{v}_F}{v_F} + g_i \frac{\vec{v} \cdot \vec{v}_F}{v_F^2} \frac{\vec{v}_F}{v_F} \right], \quad (31)$$

where

$$g_i = 1 + \frac{k_i}{c_{0i}} v_F = \frac{1}{c_{0i}} \left[ \frac{1}{\sqrt{\pi}} \left( \frac{1}{s_{0i}} - \frac{3}{2s_{0i}^3} \right) e^{-s_{0i}^2} + \left( 1 - \frac{1}{s_{0i}^2} + \frac{3}{4s_{0i}^4} \right) \text{erf}(s_{0i}) \right]. \quad (32)$$

Eq. (31) was already used in Pástor (2012b) to derive the secular time derivatives of the Keplerian orbital elements caused by the IGF.

## 5. The equation of motion

Since we want to study the motion of a dust particle in the frame of reference associated with the star in the planar CR3BP, we must add to the sum of Eqs. (21), (22), and (24), the corresponding gravitational accelerations. If we assume that  $(\eta/\bar{Q}'_{\text{pr}})(u/c) \ll 1$ , the equation of motion of the particle has the form

$$\begin{aligned} \frac{d\vec{v}}{dt} = & - \frac{\mu}{r^2} (1 - \beta) \vec{e}_R - \frac{G_0 M_P}{|\vec{r} - \vec{r}_P|^3} (\vec{r} - \vec{r}_P) - \frac{G_0 M_P}{r_P^3} \vec{r}_P \\ & - \beta \frac{\mu}{r^2} \left( 1 + \frac{\eta}{\bar{Q}'_{\text{pr}}} \right) \left( \frac{\vec{v} \cdot \vec{e}_R}{c} \vec{e}_R + \frac{\vec{v}}{c} \right) \\ & - \sum_i c_{Di} \gamma_i |\vec{v} - \vec{v}_F| (\vec{v} - \vec{v}_F). \end{aligned} \quad (33)$$

Eq. (33) can be numerically solved in order to obtain the motion of the dust particle.

## 6. Averaged resonant equations for the non-gravitational effects considered

Because we assume that the electromagnetic radiation and radial stellar wind are independent of the direction from the star (spherical symmetry), the secular variations of any given particle orbit are independent of the spatial orientation of the orbit for the accelerations caused by the PR effect and radial stellar wind. Therefore, for the PR effect and radial stellar wind, the theory presented in Beugé & Ferraz-Mello (1993) can be used. However, the secular variations of the particle orbit for the acceleration caused by an IGF depend on the orientation of the orbit with respect to the IGF velocity vector and in this case the theory developed in Sec. 2 can be used. The last term in Eq. (33) does not allow directly determining the secular variations of the particle orbit caused by the IGF in a finite analytical form. Hence, in analytical calculations, we will use Eq. (31) instead

of Eq. (24). Thus, the non-conservative part of the acceleration in Eq. (1) is

$$\begin{aligned} \vec{Y} = & -\beta \frac{\mu}{r^2} \left( 1 + \frac{\eta}{\bar{Q}'_{\text{pr}}} \right) \left( \frac{\vec{v} \cdot \vec{e}_{\text{R}}}{c} \vec{e}_{\text{R}} + \frac{\vec{v}}{c} \right) \\ & - \sum_i c_{0i} \gamma_i v_{\text{F}}^2 \left[ \frac{\vec{v}}{v_{\text{F}}} - \frac{\vec{v}_{\text{F}}}{v_{\text{F}}} + g_i \frac{\vec{v} \cdot \vec{v}_{\text{F}}}{v_{\text{F}}^2} \frac{\vec{v}_{\text{F}}}{v_{\text{F}}} \right]. \end{aligned} \quad (34)$$

We calculated the average values of  $Q_i$  and  $P_i$  in Eqs. (6) using the assumption that the temperature, concentration, and velocity of all gas components in the IGF are constant. The results for the averaged non-conservative terms in Eqs. (12) are

$$\begin{aligned} \langle Q_1 \rangle &= - \sum_i \frac{3c_{0i} \gamma_i v_{\text{F}} a e S}{L} + (1 - \alpha) \langle Q_2 \rangle, \\ \langle Q_2 \rangle &= \sum_i \frac{c_{0i} \gamma_i v_{\text{F}} a \alpha S}{2L} \left\{ \frac{3}{e} - \frac{\sigma g_i I}{v_{\text{F}}} \left[ \frac{2\alpha^2}{(1 + \alpha)^2} - 1 \right] \right\}, \\ \langle P_1 \rangle &= -\frac{\beta \mu n}{2c\alpha^3} \left( 1 + \frac{\eta}{\bar{Q}'_{\text{pr}}} \right) (3e^2 + 2) - \sum_i c_{0i} \gamma_i v_{\text{F}}^2 \sigma a \alpha \left[ 1 + \frac{g_i (S^2 + \alpha I^2)}{v_{\text{F}}^2 (1 + \alpha)} \right], \\ \langle P_2 \rangle &= -\langle P_1 \rangle - \frac{\beta \mu n}{c} \left( 1 + \frac{\eta}{\bar{Q}'_{\text{pr}}} \right) - \sum_i c_{0i} \gamma_i v_{\text{F}}^2 a \left[ \frac{3eI}{2v_{\text{F}}} + \sigma \alpha^2 \left( 1 + \frac{g_i}{2} \right) \right], \end{aligned} \quad (35)$$

where

$$\sigma = \frac{1}{v_{\text{F}}} \sqrt{\frac{\mu(1 - \beta)}{a(1 - e^2)}}, \quad (36)$$

$$\begin{aligned} S &= v_{\text{F1}} \cos \tilde{\omega} + v_{\text{F2}} \sin \tilde{\omega}, \\ I &= -v_{\text{F1}} \sin \tilde{\omega} + v_{\text{F2}} \cos \tilde{\omega}, \end{aligned} \quad (37)$$

with the Cartesian coordinates of the interstellar gas flow velocity vector denoted by  $v_{Fk}$ . An equivalent way of obtaining Eqs. (35) is to use the following identities in Eqs. (15):

$$\begin{aligned}
\left\langle \frac{da}{dt} \right\rangle_{\text{EF}} &= -\frac{\beta\mu}{ca\alpha^3} \left( 1 + \frac{\eta}{\bar{Q}'_{\text{pr}}} \right) (2 + 3e^2) \\
&\quad - \sum_i \frac{2c_{0i}\gamma_i v_{\text{F}}^2 \sigma a^2 \alpha}{L} \left[ 1 + \frac{g_i (S^2 + \alpha I^2)}{v_{\text{F}}^2 (1 + \alpha)} \right], \\
\left\langle \frac{de}{dt} \right\rangle_{\text{EF}} &= -\frac{\beta\mu}{2ca^2\alpha} \left( 1 + \frac{\eta}{\bar{Q}'_{\text{pr}}} \right) 5e \\
&\quad + \sum_i \frac{c_{0i}\gamma_i v_{\text{F}} a \alpha}{2L} \left[ 3I + \frac{\sigma g_i \alpha^2 (1 - \alpha) (I^2 - S^2)}{v_{\text{F}} e (1 + \alpha)} \right], \\
\left\langle \frac{d\tilde{\omega}}{dt} \right\rangle_{\text{EF}} &= \sum_i \frac{c_{0i}\gamma_i v_{\text{F}} a \alpha S}{2L} \left\{ -\frac{3}{e} + \frac{\sigma g_i I}{v_{\text{F}}} \left[ \frac{2\alpha^2}{(1 + \alpha)^2} - 1 \right] \right\}, \\
\left\langle \frac{d\sigma_{\text{b}}}{dt} + t \frac{dn}{dt} \right\rangle_{\text{EF}} &= \sum_i \frac{c_{0i}\gamma_i v_{\text{F}} a S}{2L} \left\{ \frac{3(1 + e^2)}{e} - \frac{\sigma g_i \alpha^2 I}{v_{\text{F}}} \left[ \frac{2\alpha^2}{(1 + \alpha)^2} - 1 \right] \right\}. \tag{38}
\end{aligned}$$

The first three equations in Eqs. (38) were already obtained in Pástor (2012b) in a slightly different, but equivalent, form. In the first equation we can see that the semimajor axis is always a decreasing function of time. Hence, the particles can migrate into MMRs from larger values of semimajor axes. The evolution of particle's Keplerian orbital elements under the action of the considered non-gravitational effects in the planar case (when the interstellar gas flow velocity lies in the orbital plane of the particle) without the gravitational influence of a planet is characterized by non-monotonic variations in the orbital eccentricity. The eccentricity can commonly reach values larger than 0.5 and then can again decrease to values close to zero (Pástor, Klačka & Kómar 2011; Pástor 2012a). At the values of eccentricity close to zero the dust particle can be captured into MMRs more efficiently. Detailed analysis of capture probability at the values of eccentricity larger than 0.5 is beyond the scope of this paper. However, we will return to this open problem in Sec. 8.

The time derivative of the orbit eccentricity averaged over the resonant libration period of the semimajor axis, obtained from Eq. (18) or Eq. (20), for the considered effects, is

$$\begin{aligned}
\left\langle \frac{de}{dt} \right\rangle &= \frac{\beta\mu\alpha}{ca^2e} \left( 1 + \frac{\eta}{\bar{Q}'_{\text{pr}}} \right) \left( 1 - \frac{2 + 3e^2}{2\alpha^3} \frac{p + q}{p} \right) \\
&\quad + \sum_i \frac{c_{0i}\gamma_i v_{\text{F}}^2 a \alpha}{L} \left\{ \frac{3}{2} \frac{I}{v_{\text{F}}} + \frac{\sigma\alpha^2}{e} \left( 1 + \frac{g_i}{2} \right) \right. \\
&\quad \left. - \frac{\sigma\alpha}{e} \left[ 1 + \frac{g_i (S^2 + \alpha I^2)}{v_{\text{F}}^2 (1 + \alpha)} \right] \frac{p + q}{p} \right\}. \tag{39}
\end{aligned}$$

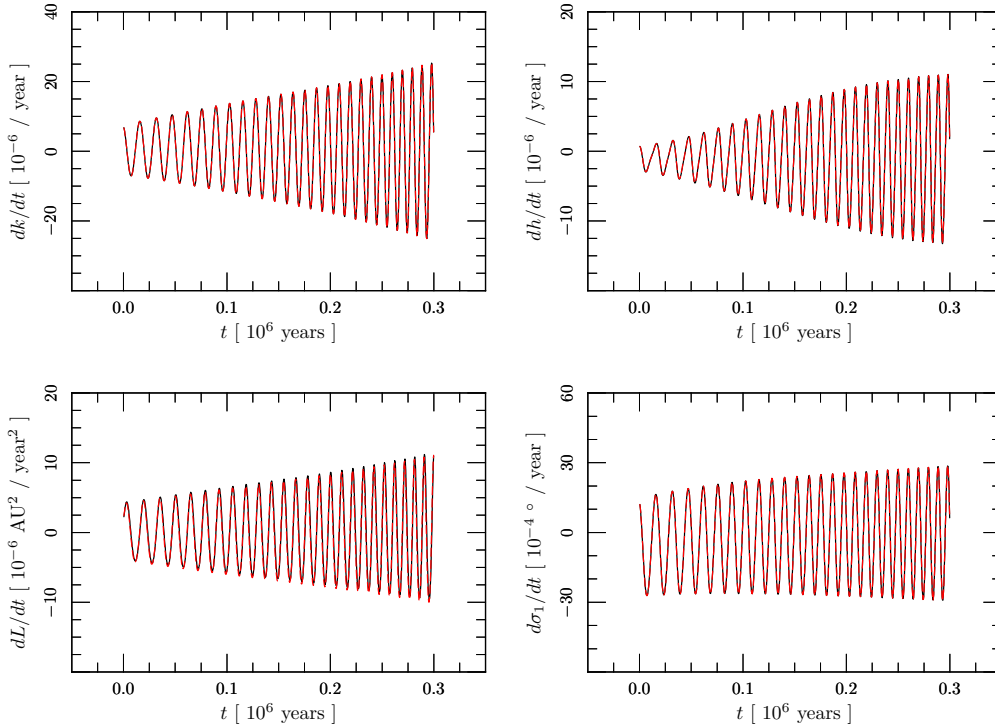


Fig. 1.— Comparison of the time derivatives of  $k$ ,  $h$ ,  $L$  and  $\sigma_1$ , averaged over the synodic period, obtained from the numerical solution of the equation of motion (solid black line) and from the analytical theory (dashed red line) for a dust particle with  $R = 2 \mu\text{m}$ ,  $\rho = 1 \text{ g/cm}^3$ , and  $\bar{Q}'_{\text{pr}} = 1$  captured in an exterior mean motion orbital 2/1 resonance with Neptune under the action of the PR effect, the radial solar wind, and the IGF.

Fig.	$a_{\text{in}}$ [ AU ]	$e_{\text{in}}$ [ - ]	$\tilde{\omega}_{\text{in}}$ [ $^\circ$ ]	$f_{\text{in}}$ [ $^\circ$ ]
2	$a_{2/1} + 0.001$	0.6	295	0
3	$a_{2/1} + 0.001$	0.5	0	0
4	$a_{2/1} + 0.001$	0.5	90	0

Table 1: The initial conditions of the dust particle for the numerical solutions of the equation of motion of which the results were depicted in Figs. 2, 3 and 4.

## 7. Comparison of the analytical and numerical results

Interstellar gas penetrates also into the heliosphere and can affect the motion of dust particles in the outer parts of the Solar system. The IGF in the Solar system arrives from the direction  $\lambda_{\text{ecl}} = 254.7^\circ$  (heliocentric ecliptic longitude) and  $\beta_{\text{ecl}} = 5.2^\circ$  (heliocentric ecliptic latitude; Lallement et al. 2005). The IGF contains mainly hydrogen and helium atoms. Some of the atoms are ionized.

The ionized hydrogen in the IGF can acquire electrons from interstellar  $\text{H}^\circ$  in the outer heliosheath during the passage into the heliopause (Frisch et al. 2009; Alouani-Bibi et al. 2011). Therefore, there are two populations of neutral interstellar hydrogen inside the heliopause. The primary population comprises the original neutral hydrogen atoms of the IGF which penetrated into the heliopause. The secondary population is created by charge exchange in the outer heliosheath (between the bow shock and the heliopause). Neutral atoms from both the primary and the secondary population penetrate freely inside the heliopause. The solar wind concentration decreases as  $r^{-2}$  inside the heliopause. Thus, the efficiency of charge exchange is reduced dramatically as compared with the efficiency in front of the heliopause, and the two populations flow through the inner heliosheath practically without any change (Frisch et al. 2009). We neglect the influences of solar gravity and solar radiation pressure on the motion of the neutral hydrogen inside the heliopause, which is important only a few AUs from the Sun. For the same reason, we also neglect any losses of neutral hydrogen due to ionization by the solar wind and the solar extreme ultraviolet radiation inside the heliopause. Neutral interstellar helium flows freely through the outer heliosphere (with only  $\leq 2\%$  filtration through charge exchange with  $\text{H}^+$ ) and inside of the Earth’s orbit is ionized by photoionization and electron ionization (Frisch et al. 2009). We assume that the temperatures, concentrations, and velocities of both populations of the neutral hydrogen and the neutral helium can be approximated by constant values. To see that this approximation is usable, we refer the reader to Alouani-Bibi et al. (2011).

The velocity vector of the IGF in the Solar system does not lie exactly in Neptune’s orbital plane. The angle between the direction of the velocity vector of the interstellar gas and Neptune’s orbital plane is  $3.7^\circ$ . The obtained orbital evolutions of the dust particles under the action of the PR effect, the radial solar wind, and the IGF are almost indistinguishable from the coplanar case due to the small value of this angle (Pástor, Klačka & Kómar 2011). This can be understood using the secular time derivatives of the orbital elements for an arbitrary orientation of the orbit caused by the considered effects. The secular time derivatives are shown in Pástor (2012b). The secular time derivative of the inclination caused by the PR effect and the radial solar wind is zero, and the secular time derivative of inclination caused by the IGF is proportional to the component of the velocity vector of the interstellar gas that is normal to the particle’s orbital plane (in our case, approximately the orbital plane of Neptune). Because the normal component of the interstellar gas velocity vector is small, the inclination of the orbit can be approximated by a constant value (in our case, a value close to zero). The fact that the velocity vector of the IGF does not lie exactly in the orbital plane of Neptune has also a positive effect. The velocity and concentration of the IGF are not significantly affected by the Sun, because any part of Neptune’s orbital plane is not in the “shadow” cast by the Sun in the IGF. The “shadow” goes beneath Neptune’s orbital plane.

We adopted the following concentrations and temperatures for various components in the IGF.  $n_1 = 0.059 \text{ cm}^{-3}$  and  $T_1 = 6100 \text{ K}$  for the primary population of neutral hydrogen (Frisch et al. 2009),  $n_2 = 0.059 \text{ cm}^{-3}$  and  $T_2 = 16500 \text{ K}$  for the secondary population of neutral hydrogen (Frisch et al. 2009), and  $n_3 = 0.015 \text{ cm}^{-3}$  and  $T_3 = 6300 \text{ K}$  for the neutral helium (Lallement et al. 2005).

The assumed interstellar gas speed is equal for all components and identical to the speed of the neutral helium entering the Solar system,  $v_F = 26.3 \text{ km s}^{-1}$  (Lallement et al. 2005). The IGF velocity vector was rotated into Neptune’s orbital plane around an axis lying in Neptune’s orbital plane and perpendicular to the velocity vector of the interstellar gas, in order to ensure the validity of the planar case in our numerical investigations.

To compare the analytical and numerical results, we considered a dust particle with  $R = 2 \text{ }\mu\text{m}$ ,  $\varrho = 1 \text{ g/cm}^3$ , and  $\bar{Q}'_{\text{pr}} = 1$ . We neglected the Lorentz force, which is only important for submicrometer particles (Dohnanyi 1978; Leinert & Grün 1990; Dermott et al. 2001). The interval between collisions is on the order of  $10^7$  years for a particle with  $R = 2 \text{ }\mu\text{m}$  beyond the orbit of Neptune (Pástor, Klačka & Kómar 2011). We assumed that the atoms are specularly reflected at the surface of the dust grain ( $\delta_i = 1$  in Eq. 25), and we used the approximation that the drag coefficients are constant ( $c_{D_i} = c_{D_i}(s_{0_i})$  and  $g_i = 1$ ). The approximation that the drag coefficients are constant is usable if the inequality  $|\vec{v}| \ll v_F$  holds during an orbit (for a comparison of the evolutions, see Fig. 5 in Pástor 2012b). The time derivatives of the parameters  $k$ ,  $h$ ,  $L$ , and  $\sigma_1$ , averaged over a synodic period, obtained from a numerical solution of Eq. (33) (solid black line) and from analytical relations given by Eqs. (12) (dashed red line) are compared in Fig. 1. The planet was initially located on the positive  $x$ -axis. The initial semimajor axis of the dust particle for the numerical solution of equation of motion is computed from the relation  $a_{\text{in}} = a_{n_P/n} + \Delta$ , where  $a_{n_P/n} = a_P (1 - \beta)^{1/3} (n_P/n)^{2/3}$  (with the assumption that  $M_P \ll M_\star$ ) and  $\Delta$  is a shift from the exact resonant semimajor axis. As the initial conditions for the dust particle we used  $a_{\text{in}} = a_{2/1} + 0.001 \text{ AU}$ ,  $e_{\text{in}} = 0.2$ ,  $\tilde{\omega}_{\text{in}} = 285^\circ$ . The initial true anomaly of the dust particle was  $f_{\text{in}} = 0^\circ$ . On the right-hand sides of Eqs. (12) we used the numerically calculated values of  $k$ ,  $h$ ,  $L$ ,  $a$ ,  $e$  and  $\tilde{\omega}$  averaged over the synodic period. The terms  $\partial R/\partial a$ ,  $\partial R/\partial e$ , and  $\partial R/\partial \tilde{\omega}$  averaged over the synodic period were calculated from their definition given by Eq. (8).  $\partial R/\partial k$  and  $\partial R/\partial h$  in Eqs. (12) were calculated from Eqs. (14) using  $\partial R/\partial e$  and  $\partial R/\partial \sigma_0$ . As can be seen in Fig. 1, the numerical and analytical results are in excellent agreement.

## 8. Types of orbits

The evolution in the  $kh$  plane is found to be an ideal tool for determining the types of orbits. The main property of this plane is its division into sets by a line on which collisions of the planet and the particle take place. The collisions line, for the exterior mean motion orbital 2/1 resonance, is depicted in Figs. 2, 3, and 4 by a dashed line. For this resonance, the phase space is practically divided into two sets. We will refer to the first set as the region below the collision curve (low-eccentricity region) and the second set as the region beyond the collision curve. The evolutions in the region below the collision curve are depicted in Figs. 2 and 4. One evolution from the region beyond the collision curve is shown in Fig. 3. We used the same parameters for the dust particle and the non-gravitational effects as in Sec. 7. The evolutions depicted are from left to right and from top to bottom:  $a$  (semimajor axis),  $e$  (eccentricity),  $\tilde{\omega}$  (longitude of perihelion),  $C_T$



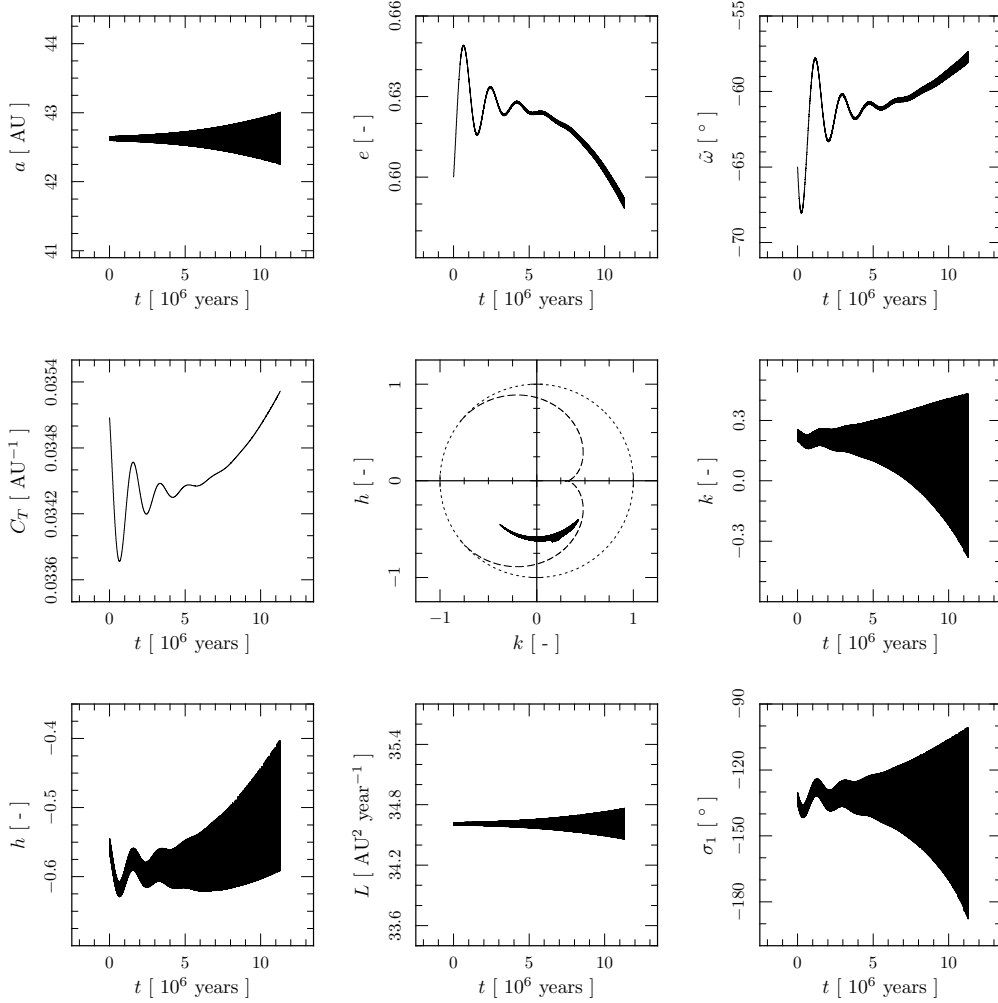


Fig. 2.— The evolutions of parameters described in the text for a dust particle with  $R = 2 \mu\text{m}$ ,  $\rho = 1 \text{ g/cm}^3$ , and  $\bar{Q}'_{\text{pr}} = 1$  captured in an exterior mean motion orbital 2/1 resonance with Neptune under the action of the PR effect, the radial solar wind, and the IGF. In the  $kh$  plane, the resonant libration occurs around the bottom libration center of the conservative problem. The evolutions of eccentricity and longitude of perihelion during libration around this center have damped oscillations approaching some relatively slowly changing values.

$= (1 - \beta)/(2a) + \sqrt{(1 - \beta)a(1 - e^2)/a_{\text{P}}^3}$  (Tisserand parameter),  $kh$  point,  $k = e \cos \sigma_0$ ,  $h = e \sin \sigma_0$ ,  $L = \sqrt{\mu(1 - \beta)a}$ , and  $\sigma_1 = (p + q)\lambda_{\text{P}}/q - p\lambda/q$ . All parameters are averaged over the synodic period. We must note that the evolution duration  $11.3 \times 10^6$  years (Fig. 2) requires the size of an interstellar gas cloud 303.9 pc in the direction of the interstellar gas velocity vector (constant velocity with magnitude  $26.3 \text{ km s}^{-1}$  is assumed) and such a situation cannot always occur in the real Galactic environment. Evolutions with such long capture times should be used only for

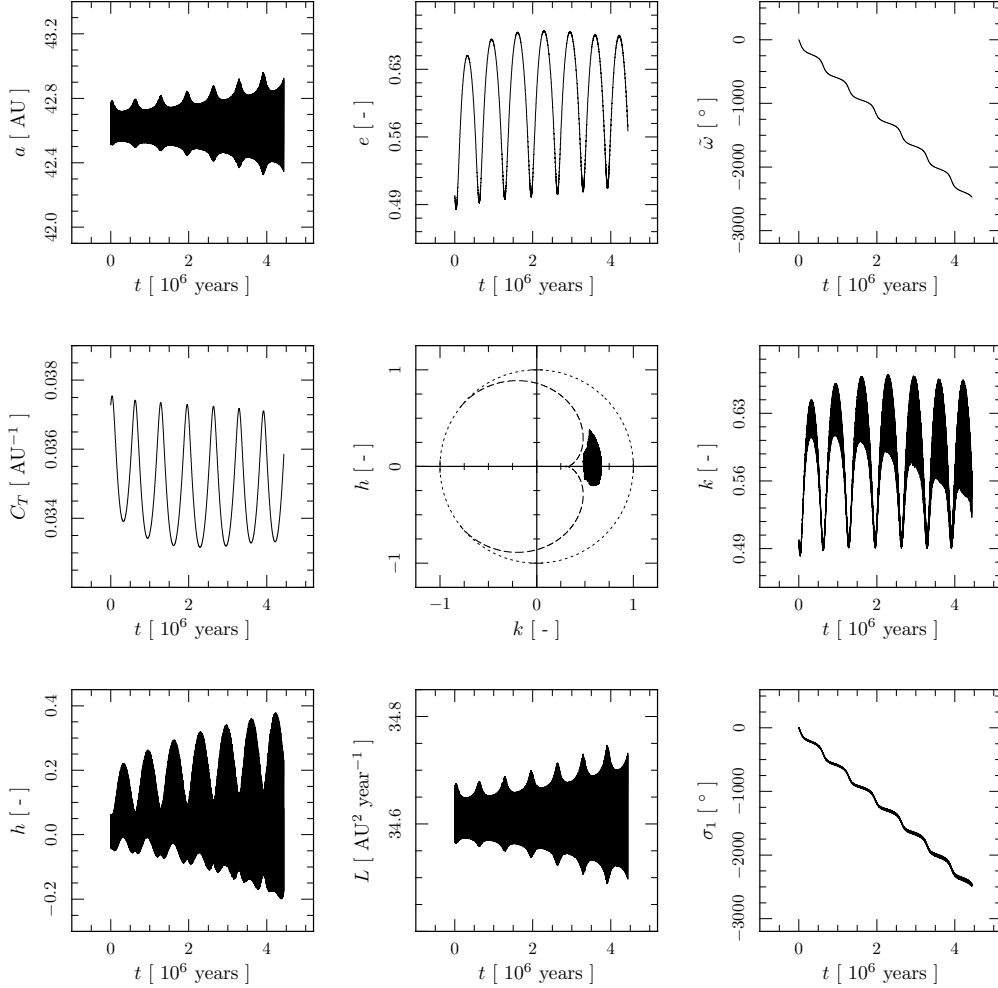


Fig. 3.— The same dust particle, resonance, and non-gravitational effects as in Fig. 2, but in this case the resonance libration occurs around the libration center of the conservative problem which is located on the right side of the origin in the  $kh$  plane. The orbital evolutions with libration around this center have oscillations in the eccentricity and a fast monotonic advance of the longitude of perihelion.

theoretical purposes. A shorter part of the evolution is still valid. The planet was initially located on the positive  $x$ -axis. The initial conditions of the dust particle are in Table 1. We used the numerical integrations of the equation of motion to decide if for the values of eccentricity close to 0.5 (used as the initial eccentricities) is possible to capture the dust particle into an exterior mean motion orbital 2/1 resonance with Neptune under the action of the considered non-gravitational effects or not. We found that the particle can be captured into the 2/1 commensurability even for larger eccentricities. However, the capture probability for the larger eccentricities is smaller than for the eccentricities close to zero.

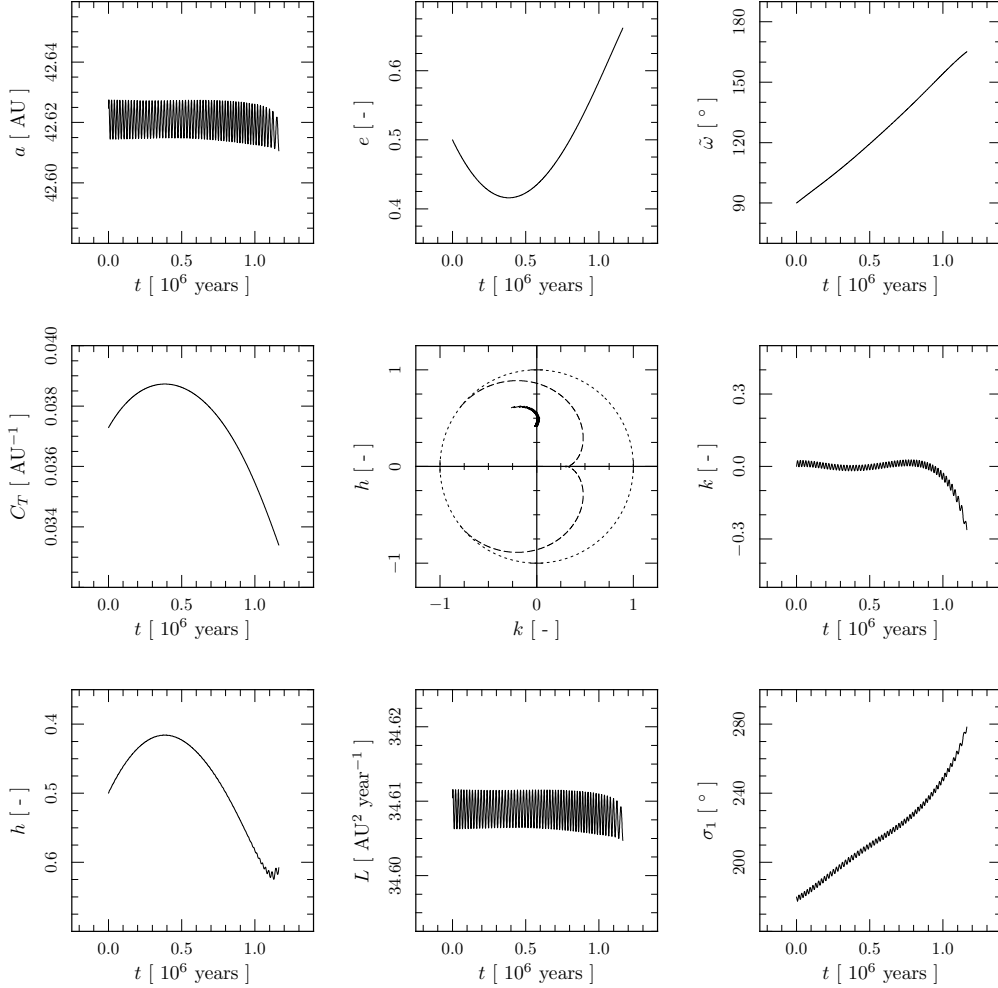


Fig. 4.— The same dust particle, resonance, and non-gravitational effects as in Figs. 2 and 3, but a capture with the resonant libration around the top libration center of the conservative problem in the  $kh$  plane is depicted in this case.

An evolution in the region beyond the collision curve correspond to a libration around one of libration centers of the conservative problem, which is located on the right of the origin on the  $h$ -axis. The orbital evolutions in the region beyond the collision curve have a fast monotonic advance of the perihelion and oscillations of the eccentricity (Fig. 3).

The orbital evolutions in the region below the collision curve can be divided into two groups, corresponding to two libration centers of the conservative problem. One evolution with a libration around the center located below the  $h$ -axis (bottom center) is depicted in Fig. 2 and one evolution with a libration around the center located above the  $h$ -axis (top center) in Fig. 4. The evolutions of eccentricity and longitude of perihelion during the libration around the bottom center have

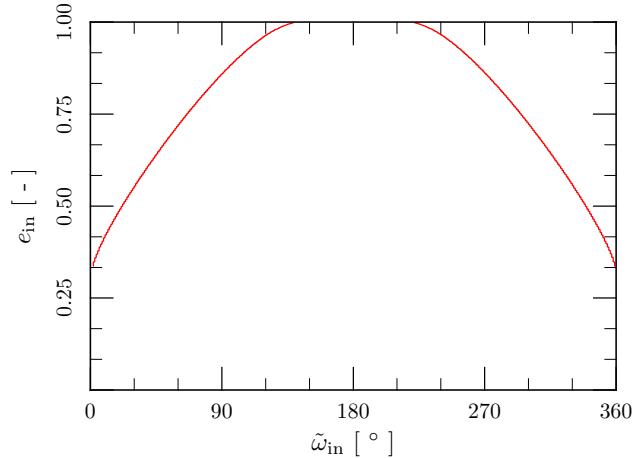


Fig. 5.— In the case when a planet in a circular orbit is initially located on the positive  $x$ -axis and a dust particle with  $R = 2 \mu\text{m}$ ,  $\rho = 1 \text{ g/cm}^3$ , and  $\bar{Q}'_{\text{pr}} = 1$  is initially in the perihelion, the depicted curve corresponds to the initial longitudes of perihelion and eccentricities of the particle leading to collisions of the planet with the particle for the exact exterior mean motion orbital 2/1 resonance.

damped oscillations approaching some “constant” values. We found that these values are not exactly constant, but they are relatively slowly changing in comparison with the evolution before this “stabilization” (as can be seen in Fig. 2).

To compare the maximal capture times for evolutions corresponding to the various libration centers of the conservative problem, we divided the initial eccentricity, longitude of perihelion, true anomaly of the particle, and true anomaly of the planet equally within the allowed intervals for the exterior mean motion orbital 2/1 resonance. The number of captures and the maximal capture times which we found for the various libration centers were different. The orbital evolutions with the libration around the bottom center have larger maximal capture times than the evolutions with the libration around the top center. This is different from the conservative problem, where both libration centers are symmetric with respect to the  $h$ -axis Beaugé (1994) and also have equal maximal capture times. We found that a horseshoe-like libration between the top and the bottom libration centers in the region below the collision curve is also possible with smaller maximal capture times.

The two groups with the largest maximal capture times (libration in the region beyond the collision curve and libration around the bottom center) were already identified in Pástor (2013). For a planet initially located on the positive  $x$ -axis and a particle with initial conditions  $a_{\text{in}} = a_{2/1}$ ,  $e_{\text{in}}$  arbitrary,  $\tilde{\omega}_{\text{in}}$  arbitrary, and  $f_{\text{in}} = 0^\circ$ , we obtain, in the  $\tilde{\omega}_{\text{in}}e_{\text{in}}$  plane, the collision line depicted in Fig. 5. This curve divides the evolutions in Pástor (2013) into two groups (in the present paper, we refer to these two groups as the region below the collision curve and the region beyond the collision curve).

### 9. Conditions for stable orbits

Eqs. (12) enable searching for stable orbits determined by

$$\frac{dk}{dt} = \frac{dh}{dt} = \frac{dL}{dt} = 0 . \quad (40)$$

Equations (40) are conditions for stability in a synodic period. This should not be understood in the sense that if the conditions hold, then an orbit will be stable during an arbitrary time interval. The stability is obtained only in the synodic period. However, in an exact resonance due to periodical repeating of relative positions of the planet and the dust particle the validity of the conditions implies that the orbit will be stable during the arbitrary time interval (during which the conditions hold). The evolution in the synodic period will be repeated periodically. We must note that in reality other small forces can destroy the exact periodicity. The evolution shown in Fig. 2 clearly does not represent a stable solution determined by Eqs. (40) because  $k$  and  $h$  rapidly change during the evolution. Substitution of Eqs. (40) in Eqs. (12) leads to the conditions

$$\begin{aligned} \langle P_1 \rangle - s \langle P_2 \rangle &= 0 , \\ e \frac{\partial R}{\partial e} &= k \frac{\partial R}{\partial k} + h \frac{\partial R}{\partial h} = \frac{Le^2}{\alpha} \left( \frac{d\sigma_1}{dt} + \langle Q_2 \rangle \right) , \\ \frac{\partial R}{\partial \sigma_0} &= k \frac{\partial R}{\partial h} - h \frac{\partial R}{\partial k} = \langle P_2 \rangle . \end{aligned} \quad (41)$$

The first equation in Eqs. (41) is equivalent with the condition  $\langle de/dt \rangle = 0$  (Eq. 20).

Eqs. (41) describe also stable orbits with  $d\sigma_1/dt \neq 0$ , in general. Now we show that such stable orbits are not possible under the action of the considered non-gravitational effects. The second equation of Eqs. (41) can be rewritten using the second equation of Eqs. (15) and the last equation of Eqs. (13) as follows:

$$e \frac{\partial R}{\partial e} = \frac{Le^2}{\alpha} \left( \frac{d\sigma_1}{dt} - \frac{d\tilde{\omega}}{dt} + \frac{\alpha}{Le} \frac{\partial R}{\partial e} \right) . \quad (42)$$

This equation is equivalent with the condition

$$\frac{d\sigma_0}{dt} = \frac{d\sigma_1}{dt} - \frac{d\tilde{\omega}}{dt} = 0 . \quad (43)$$

Therefore, if  $d\sigma_1/dt \neq 0$ , then the longitude of pericenter of the orbit of the particle must change. Since the eccentricity is constant for a stable orbit, we can write for the first of Eqs. (41) (see Eqs. 35)

$$B(\tilde{\omega}) = \langle P_1 \rangle - s \langle P_2 \rangle = \alpha_1 S^2 + \alpha_2 I^2 + \alpha_3 I + \alpha_4 = 0 , \quad (44)$$

where  $\alpha_p$  for  $p = 1, \dots, 4$  are some constants.  $B(\tilde{\omega})$  is constant for all  $\tilde{\omega}$  and its derivative with respect to time must be zero. We get

$$\frac{dB}{dt} = \frac{dB}{d\tilde{\omega}} \frac{d\tilde{\omega}}{dt} = (2\alpha_1 I - 2\alpha_2 I - \alpha_3) S \frac{d\tilde{\omega}}{dt} = 0 . \quad (45)$$

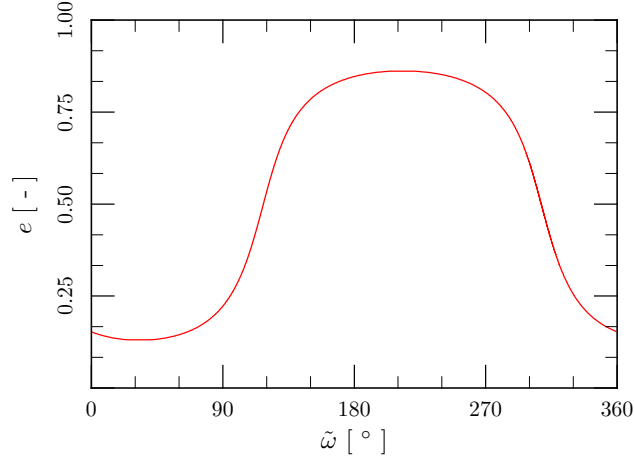


Fig. 6.— The longitudes of perihelion and the eccentricities for which the first equation of system Eqs. 47 hold for a dust particle with  $R = 2 \mu\text{m}$ ,  $\varrho = 1 \text{ g/cm}^3$ , and  $\bar{Q}'_{\text{pr}} = 1$  captured in an exterior mean motion orbital 2/1 resonance with Neptune under the action of the PR effect, the radial solar wind, and the IGF.

Because  $\alpha_1 \neq \alpha_2$  and  $\alpha_3 \neq 0$ , for all existing stable orbits there must hold

$$\frac{d\tilde{\omega}}{dt} = \frac{d\sigma_1}{dt} = 0 . \quad (46)$$

We conclude that the longitude of pericenter must be constant for all stable orbits. If we use Eq. (40) and Eq. (46) in Eqs. (12), we obtain for the considered non-gravitational effects the following conditions for stable orbits:

$$\begin{aligned} \langle P_1 \rangle - s \langle P_2 \rangle &= 0 , \\ \frac{\partial R}{\partial e} &= \frac{Le}{\alpha} \langle Q_2 \rangle , \\ \frac{\partial R}{\partial \sigma_0} &= \langle P_2 \rangle , \\ \frac{2sL}{\mu(1-\beta)} \frac{\partial R}{\partial a} &= -n_{\text{P}} \frac{p+q}{q} + ns - s \langle Q_1 \rangle + (1-\alpha) s \langle Q_2 \rangle . \end{aligned} \quad (47)$$

Solutions of this system of equations represent points in a five dimensional space with  $a_{\text{in}}$ ,  $e_{\text{in}}$ ,  $\tilde{\omega}_{\text{in}}$ ,  $f_{\text{in}}$  and  $f_{\text{P in}}$  on the axes. Here,  $f_{\text{in}}$  and  $f_{\text{P in}}$  are the initial true anomalies of the particle and the planet, respectively.

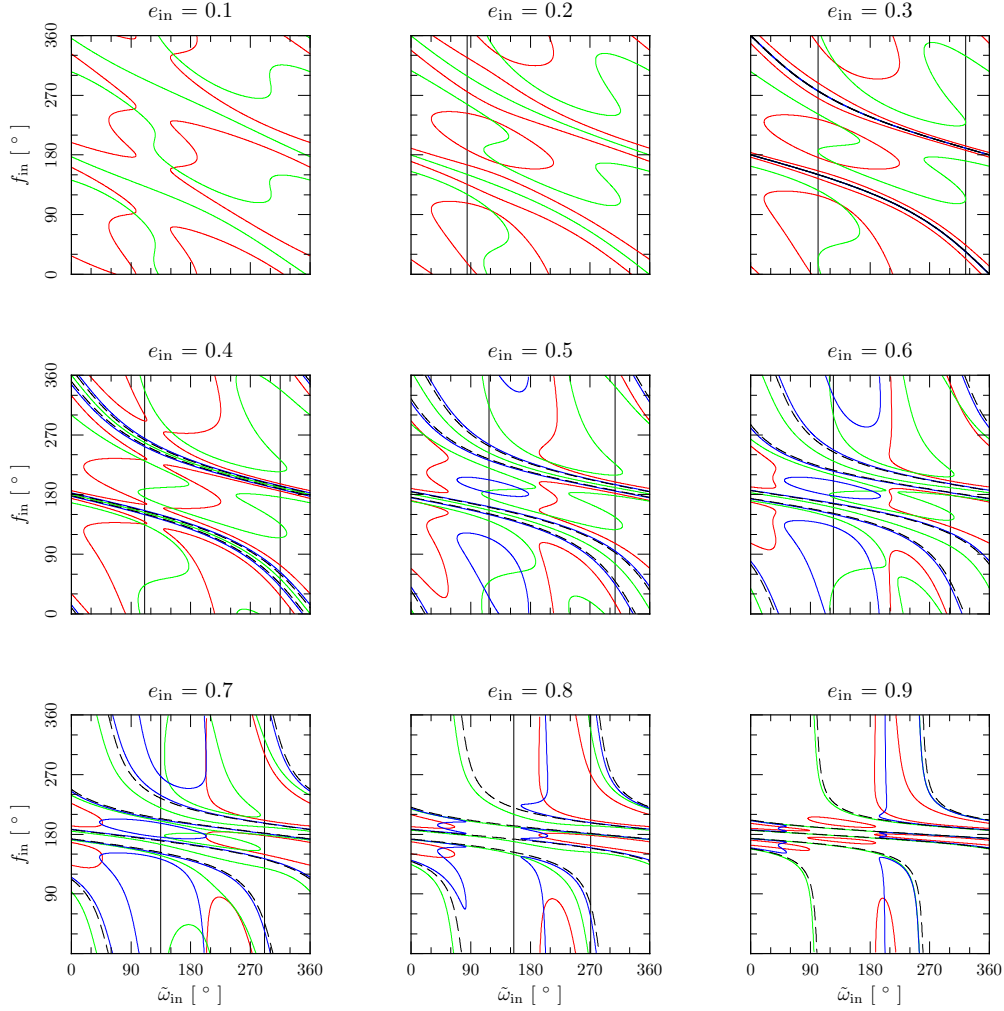


Fig. 7.— Sections of three dimensional phase space determined by solutions of the last three equations in Eqs. (47) for a dust particle with  $R = 2 \mu\text{m}$ ,  $\rho = 1 \text{ g/cm}^3$ , and  $\bar{Q}'_{\text{pr}} = 1$  captured in the exact exterior mean motion orbital 2/1 resonance with Neptune under the action of the PR effect, the radial solar wind, and the IGF. Vertical lines in a given section correspond to the longitude of perihelion for which the first equation of Eqs. (47) holds. Red, green, and blue lines correspond to solutions of the second, third, and fourth equation in Eqs. (47), respectively. Collisions of the planet with the particle occur for points on the dashed lines.

### 10. Searching for stable orbits in an exterior mean motion orbital 2/1 resonance with Neptune

Equations (47) can be used for searching of stable orbits during the synodic period. The approach can be divided into a special case of exact resonance and the more general case of non-

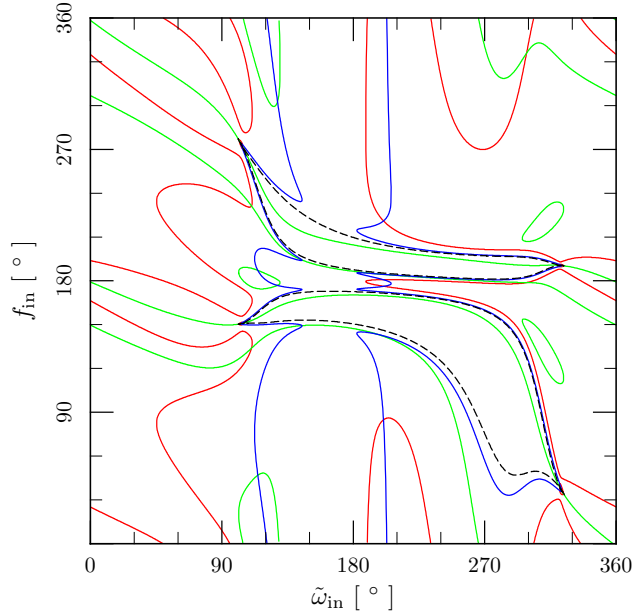


Fig. 8.— Red, green, and blue lines correspond to solutions of the second, third, and fourth equation in Eqs. (47) with substituted solutions from the first equation in Eqs. (47), respectively. Collisions of the planet with the particle occur for points on the dashed lines.

exact resonance.

### 10.1. Exact resonance

We have searched for stable orbits for a particle captured in the exact exterior mean motion orbital 2/1 resonance with Neptune under the action of the PR effect, the radial solar wind, and the IGF. The particle and the non-gravitational effects were described by the same parameters as in Sec. 7. The relation depicted in Fig. 6 represents pairs of  $\tilde{\omega}$  and  $e$  for which the first equation of Eqs. (47) holds. Any stable solution must lie on this curve. Also the secular time derivative of the eccentricity averaged over a libration period is zero for the points on the curve (Sec. 3).

As was already mentioned, the phase space of the solutions of the three remaining equations in the system of equations given by Eqs. (47) has five dimensions. For an exact resonance, the number of dimensions can be reduced. If we consider the exact resonance with  $n_{\text{P}}(p + q) = np$ , then  $a_{\text{in}}$  is determined by the condition  $a_{\text{in}} = a_{\text{P}} (1 - \beta)^{1/3} [M_{\star}/(M_{\star} + M_{\text{P}})]^{1/3} (n_{\text{P}}/n)^{2/3}$ . Due to the exact resonance, a further reduction in the number of dimensions is possible. In the exact resonance, for all initial positions of the planet and all initial positions of the dust particle, we can find the same value of the terms  $\partial R/\partial e$ ,  $\partial R/\partial \sigma_0$ , and  $\partial R/\partial a$  averaged over the synodic period for a fixed initial position of the planet and calculated initial positions of the dust particle. The last



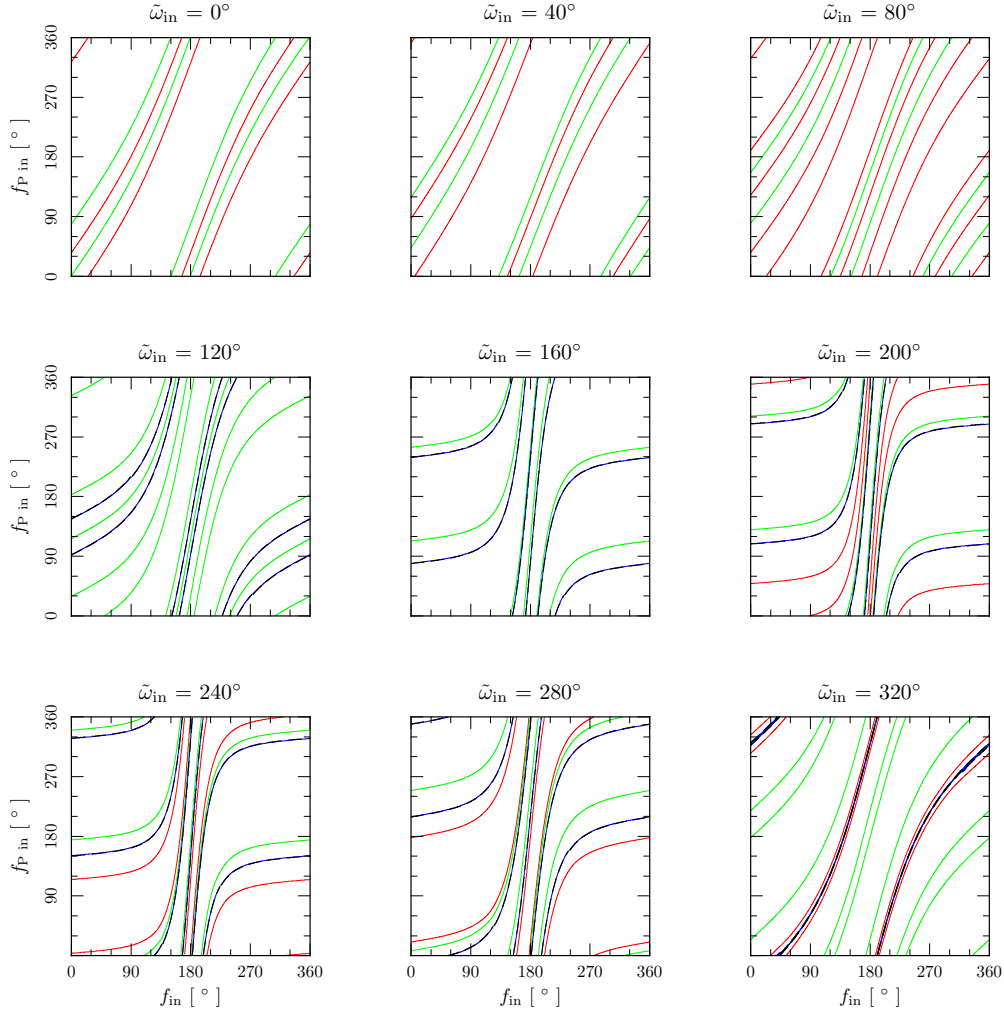


Fig. 9.— Solutions of the second (red line), third (green line) and fourth equation (blue line) with substituted solutions of the first equation in the system given by Eqs. (47) for a dust particle with  $R = 2 \mu\text{m}$ ,  $\varrho = 1 \text{ g/cm}^3$ , and  $\bar{Q}'_{\text{pr}} = 1$  captured in a non-exact exterior mean motion orbital 2/1 resonance with Neptune under the action of the PR effect, the radial solar wind, and the IGF. The shift from the exact resonance is  $\Delta = 0.075 \text{ AU}$ . Collisions of the planet with the particle occur for points on the dashed lines.

sentence can be written more mathematically in the following way. In the exact resonance holds

$$\frac{1}{T_S} \int_0^{T_S} \frac{\partial R}{\partial e} dt = \frac{1}{T_S} \left( \int_{T_A}^{T_S} \frac{\partial R}{\partial e} dt + \int_{T_S}^{T_S+T_A} \frac{\partial R}{\partial e} dt \right), \quad (48)$$

where  $T_S$  is the synodic period and  $T_A$  denotes the time in which the planet is in the fixed initial position. The validity of Eq. (48) is caused by the fact that in the exact resonance relative positions

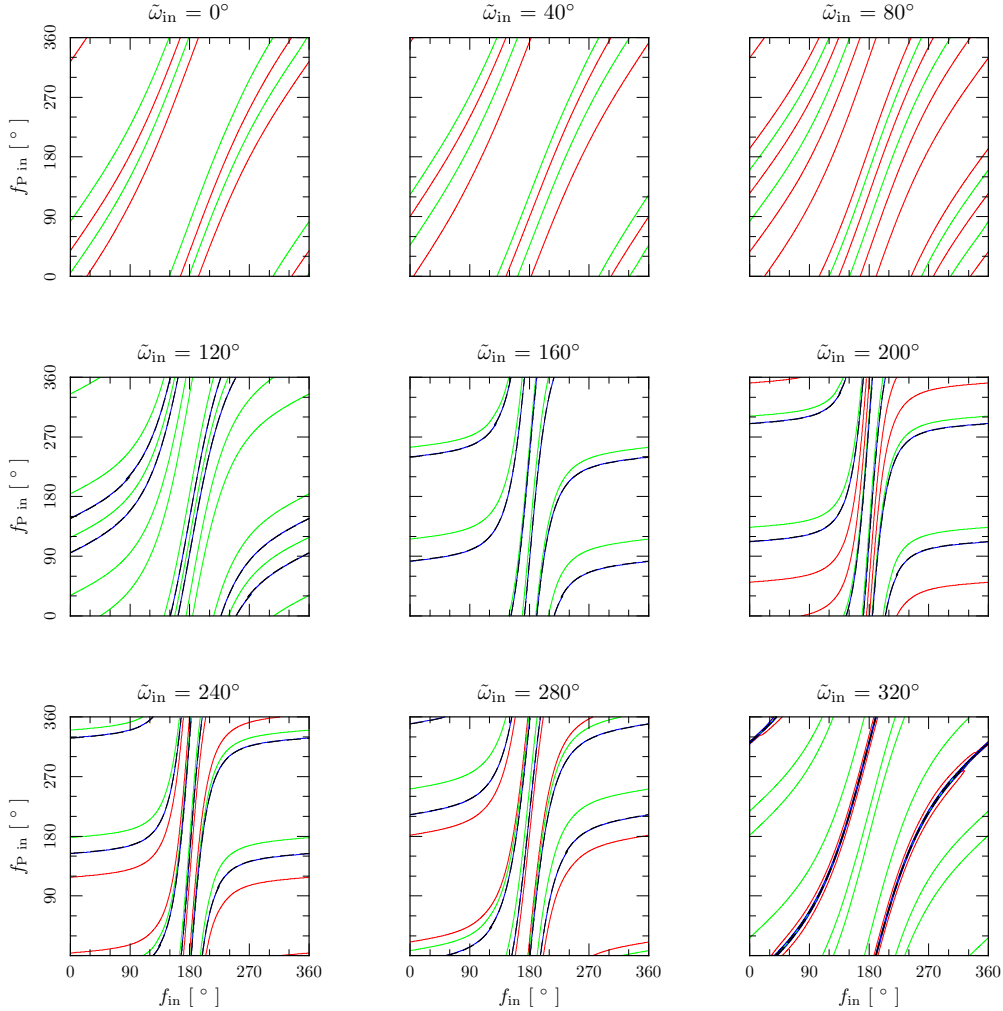


Fig. 10.— The same as in Fig. 9, but in this case the shift from the exact resonance is  $\Delta = -0.075$  AU.

of the planet and the dust particle are periodically repeating, and therefore

$$\frac{1}{T_S} \int_0^{T_A} \frac{\partial R}{\partial e} dt = \frac{1}{T_S} \int_{T_S}^{T_S+T_A} \frac{\partial R}{\partial e} dt . \quad (49)$$

Similar equations hold for  $\partial R/\partial\sigma_0$ , and  $\partial R/\partial a$ . Hence, the solutions of last three equations in the system of equations given by Eqs. (47) for the exact resonance represent points in a three dimensional space with  $e_{\text{in}}$ ,  $\tilde{\omega}_{\text{in}}$ , and  $f_{\text{in}}$  on the axes. Sections of this phase space are shown for nine different initial eccentricities in Fig. 7. The fixed initial position of the planet was on the positive  $x$ -axis. The red, green, and blue points correspond to solutions of the second, third, and fourth equation in Eqs. (47), respectively. Any point on the dashed curves in Fig. 7 leads to a collision of the planet with the particle. The perihelion distance is larger than the radius of planet’s orbit for

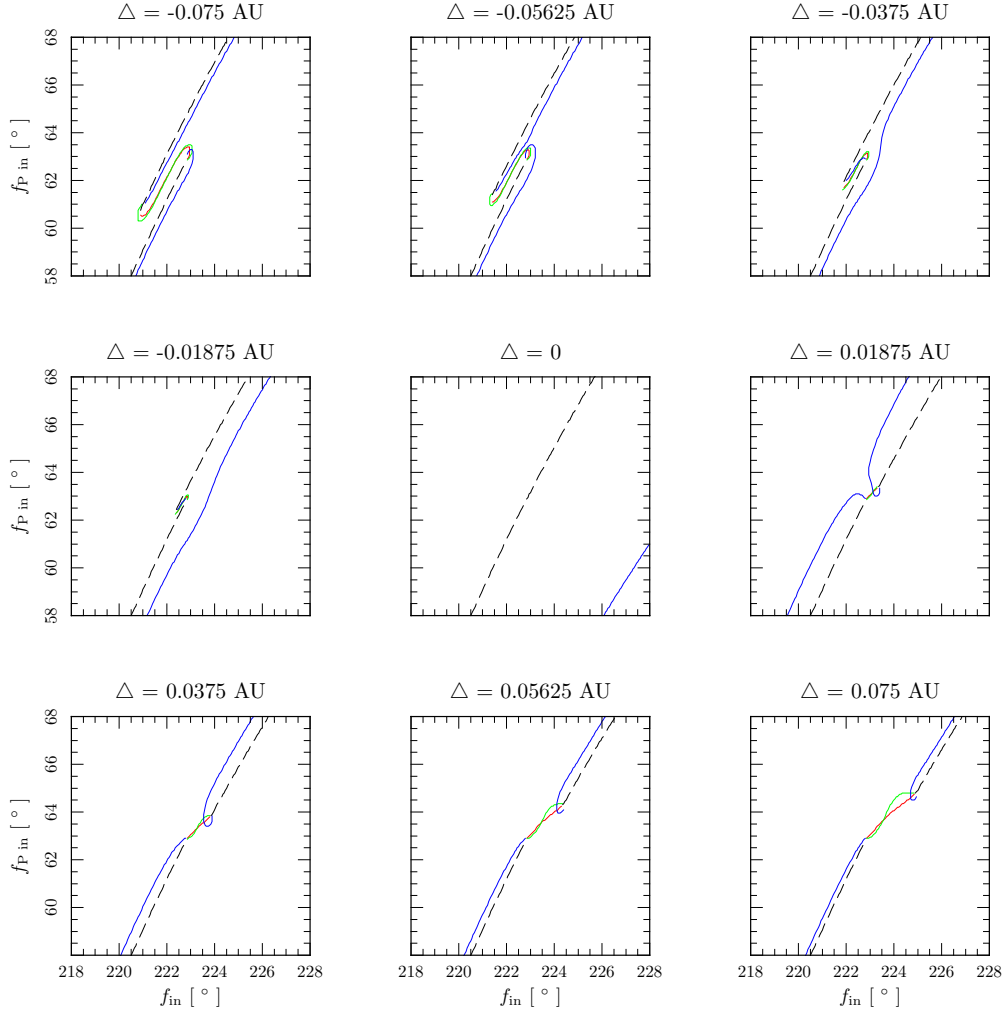


Fig. 11.— A region in  $f_{\text{in}}f_{\text{P in}}$  plane obtained with  $\tilde{\omega}_{\text{in}} = 200^\circ$ . The region is centered on the initial conditions that directly lead to a collision for  $\Delta = 0$  AU. The same situation as in Figs. 9 and 10 is solved, but in this case various values of the shift in an arithmetic sequence are used.

$e_{\text{in}} \lesssim 0.2945$ . Therefore, the dashed lines are not on the sections with initial eccentricity equal to 0.1 and 0.2. Since the planet's initial position is fixed, for every orbit with  $e_{\text{in}} \gtrsim 0.2945$ , there exist some true anomalies of the particle which lead to a collision. The vertical lines in a given section are on the positions given by the longitudes of perihelion for which the first equation of Eqs. (47) holds (see also Fig. 6). Fig. 7 allows determining the stable orbits in the exact resonance under the action of the PR effect, the radial stellar wind, and the IGF. As can be seen in Fig. 7, there is no a common point for the red, green, blue, and vertical lines. Therefore, no stable solution in Fig. 7 exists.

There also exists another way to search for stable orbits in an exact resonance with greater resolution in the initial eccentricity. We can check whether a stable orbit exists in the given problem directly for pairs of  $\tilde{\omega}_{\text{in}}$  and  $e_{\text{in}}$  determined from the first equation of Eqs. (47) and depicted in Fig. 6. The results are shown in Fig. 8. The red, green, and blue points correspond, respectively, to solutions of the second, third, and fourth equation in Eqs. (47) with substituted  $e_{\text{in}}$  obtained from the first equation of Eqs. (47). The collisions occur on the dashed curves. As can be seen in Fig. 8, the red, green, and blue lines have no common point. Therefore, similarly to Fig. 7, there does not exist any stable solution for a dust particle with  $R = 2 \mu\text{m}$ ,  $\varrho = 1 \text{ g/cm}^3$ , and  $\bar{Q}'_{\text{pr}} = 1$  captured in the exact exterior mean motion orbital 2/1 resonance with Neptune under the action of the PR effect, the radial solar wind, and the IGF.

A solution of Eqs. (47) for the exact resonance means stability during an arbitrary time interval (see comment after Eq. 40). We have three equations and only two unknowns. Due to the complicated behavior of the solutions of these equations (see Fig. 7 and 8) any dependence between the solutions is unlikely. Therefore we can say that, most probably, no stable solution exists for the exact resonance under the action of the PR effect, the radial solar wind, and the IGF.

An increase of the libration amplitude as shown in Figs. 2 and 3 suggests that there will be no stable solution in the sense described in Gomes (1995). Such a stable solution requires a constant value of eccentricity (universal eccentricity) and a decrease of the libration amplitude. As can be seen in Figs. 2 and 3, the second condition is not fulfilled for an exterior MMR with the PR effect, the radial solar wind, and the IGF. The stable solution according to Gomes (1995) converges to a zero amplitude libration. The zero amplitude libration occurs also for a stable solution in the exact resonance (see comment after Eq. 40).

## 10.2. Non-exact resonance

If the assumption about the exact resonance is not used, then four unknowns remain. We use  $a_{\text{in}}$ ,  $\tilde{\omega}_{\text{in}}$ ,  $f_{\text{in}}$ , and  $f_{\text{P in}}$ . Hence, from the first equation in Eqs. (47) we have determined  $e_{\text{in}}$ . The non-exact resonance will be created by a shift  $\Delta$  from the exact value of semimajor axis  $a_{\text{in}} = a_{\text{P}} (1 - \beta)^{1/3} [M_{\star}/(M_{\star} + M_{\text{P}})]^{1/3} (n_{\text{P}}/n)^{2/3}$ . It is reasonable to expect that the value of the semimajor axis for a stable orbit in the non-exact resonance will be in an interval of the resonant libration of semimajor axis.

We searched for the stable orbits using numerous values of the shift from the exact exterior mean motion orbital 2/1 resonance with Neptune. If we use some value of the shift, then remaining phase space of solutions is three dimensional with  $\tilde{\omega}_{\text{in}}$ ,  $f_{\text{in}}$ , and  $f_{\text{P in}}$  on the axes. Sections of this phase space for nine different longitudes of perihelion determined for  $\Delta = 0.075 \text{ AU}$  and  $\Delta = -0.075 \text{ AU}$  are shown in Fig. 9 and Fig. 10, respectively. In Fig. 2 and Fig. 3 is possible to verify that these values of the shift can be in the interval of the resonant libration of semimajor axis. We used the dust particle with  $R = 2 \mu\text{m}$ ,  $\varrho = 1 \text{ g/cm}^3$ , and  $\bar{Q}'_{\text{pr}} = 1$  under the action of the same

non-gravitational effects as in Fig. 7 and Fig. 8. Fig. 9 and Fig. 10 are depicted using the same lines types for the same solutions of the system of equations given by Eqs. (47) as in Fig. 7 and Fig. 8. For the longitudes of perihelion  $0^\circ$ ,  $40^\circ$ , and  $80^\circ$  there is no solution of the fourth equation in Eqs. (47). Solutions of the fourth equation in Eqs. (47) are in this case obtained close to the collisions of the planet with the particle and the collisions do not occur for  $e_{\text{in}} \lesssim 0.2957$  in Fig. 9 and  $e_{\text{in}} \lesssim 0.2932$  in Fig. 10.

Fig. 9 and Fig. 10 may lead to an idea that there exists a similarity between the depicted solutions of equations from the system given by Eqs. (47) for chosen values of  $\Delta$  and  $\tilde{\omega}_{\text{in}}$ . The similarity in the sense that the solutions of various equations in Eqs. (47) for chosen values of  $\Delta$  and  $\tilde{\omega}_{\text{in}}$  go always side by side. If the similarity exists, then solutions of the various equations depicted in Fig. 9 and Fig. 10 could never have a common point and no stable solution should exist. This look even more interesting if we realize that points in Fig. 8 should be obtained from Fig. 9 and Fig. 10 for  $\Delta = 0$  AU and  $f_{\text{P in}} = 0^\circ$ . In reality the similarity is obtained only for  $\Delta = 0$  AU.

The various values of  $\Delta$  in Figs. 9 and 10 lead to small shifts of the depicted curves. The greatest difference is in the plots obtained for  $\tilde{\omega}_{\text{in}} = 320^\circ$ . In these plots the depicted behavior of the red curves is different for larger values of  $f_{\text{in}}$ . For  $\tilde{\omega}_{\text{in}} = 320^\circ$  we obtain  $e_{\text{in}} \approx 0.3388$  for Fig. 9 and  $e_{\text{in}} \approx 0.3397$  for Fig. 10 from the first equation in Eqs. (47) and this is in both cases value closest to the limit value of initial eccentricity above which the collisions can occur.

The shown intervals  $[0^\circ, 360^\circ]$  for  $f_{\text{in}}$  and  $f_{\text{P in}}$  in Figs. 9 and 10 do not allow to show detailed behavior caused by  $\Delta \neq 0$  AU. Fig. 11 was created in order to show a region in which these details can be seen. The region is obtained for  $\tilde{\omega}_{\text{in}} = 200^\circ$  and various values of the shift. The same dust particle, resonance and non-gravitational effects are used as in Figs. 9 and 10. Therefore, the first and the last plot in Fig. 11 correspond to zoomed regions in the sixth plot of Fig. 10 and Fig. 9, respectively. The region is centered on initial conditions that directly lead to a collision for  $\Delta = 0$  AU. The collision occurs for  $f_{\text{in c}} \approx 222.91^\circ$  and  $f_{\text{P in c}} \approx 62.91^\circ$ . These values can be easily obtained from equations  $r = r_{\text{P}}, \cos(f_{\text{in c}} + \tilde{\omega}_{\text{in}}) = \cos f_{\text{P in c}}$  and  $\sin(f_{\text{in c}} + \tilde{\omega}_{\text{in}}) = \sin f_{\text{P in c}}$ . For the positive values of  $\Delta$  depicted in Fig. 11 there is no collision during the synodic period for  $f_{\text{in}}$  slightly larger than  $f_{\text{in c}}$  for a given plot in Fig. 11. This can be easily understood since the following inequality  $T_{\text{S}} = 2\pi q / (n - n_{\text{P}}) < 2\pi / n$  holds for  $q = -1$ . For the negative values of  $\Delta$  we obtain a second collision during the synodic period for  $f_{\text{in}}$  slightly smaller than  $f_{\text{in c}}$ .

The red, green and blue lines in Fig. 9 and Fig. 10 have no any common point. Therefore none stable solution from the initial conditions used in Fig. 9 and Fig. 10 can be obtained. It is impossible to present all the sections of the phase space given by  $a_{\text{in}}$ ,  $\tilde{\omega}_{\text{in}}$ ,  $f_{\text{in}}$ , and  $f_{\text{P in}}$  in a reasonable resolution in this paper. This phase space was carefully explored for a dust particle with  $R = 2 \mu\text{m}$ ,  $\varrho = 1 \text{ g/cm}^3$ , and  $\bar{Q}'_{\text{pr}} = 1$  captured in the exterior mean motion orbital 2/1 resonance with Neptune under the action of the PR effect, the radial solar wind, and the IGF and no stable solution was found.

## 11. Conclusion

From a near canonical form of equations of motion we derived averaged resonant equations for a circumstellar dust particle captured in an MMR with a planet in a circular orbit under the action of given non-gravitational effects in general form. The averaged resonant equations were also obtained/confirmed using Lagrange’s planetary equations. Non-gravitational effects for which the secular variations of the orbit depend on the spatial orientation of the orbit have been considered. This enabled us to investigate the motion of a dust particle in an MMR under the action of the PR effect, the radial stellar wind, and the interstellar wind. The analytically and numerically calculated averaged time derivatives of the non-canonical resonant variables are in excellent agreement. From the numerical solutions of the equation of motion, the evolutions in the  $kh$  plane can be obtained. Using the evolutions in the  $kh$  plane, the types of orbits can be easily determined. For an exterior mean motion orbital 2/1 resonance, all types of orbits correspond to libration centers of the conservative problem. From the averaged resonant equations a system of equations valid for stationary solutions can be obtained. Using the system we analytically showed that none stationary solution with an advance of pericenter exists. The obtained system can be numerically solved in order to find a stationary solution with a fixed pericenter. An exact resonance yield the phase space of solutions which has two dimensions. Since the number of remaining equations is three and some dependence between the solutions is unlikely, most probable none stationary solution in the exact resonance exists. For a non-exact resonance the phase space of solutions has four dimensions. Solutions of all three remaining equations in this phase space are very similar except for the behavior close to collisions. This similarity does not enable to obtain a stationary solution. For used test particle in the non-exact exterior 2/1 resonance under the action of the PR effect, the radial solar wind and the interstellar wind none stationary solution is located in the four dimensional phase space of solutions.

I would like to thank referees of this paper for their useful comments and suggestions.

## REFERENCES

- Alouani-Bibi F., Opher M., Alexashov D., Izmodenov V., Toth G., 2011. Kinetic versus multi-fluid approach for interstellar neutrals in the heliosphere: Exploration of the interstellar magnetic field effects. *Astrophys. J.* **734**, 45.
- Baines M. J., Williams I. P., Asebiomo A. S., 1965. Resistance to the motion of a small sphere moving through a gas. *Mon. Not. R. Astron. Soc.* **130**, 63-74.
- Belyaev M., Rafikov R., 2010. The dynamics of dust grains in the outer Solar system. *Astrophys. J.* **723**, 1718-1735.

- Bate R. R., Mueller D. D., White J. E., 1971. *Fundamentals of Astrodynamics* Dover Publications, New York
- Beauge C., 1994. Asymmetric librations in exterior resonances. *Celest. Mech. Dyn. Astron.* **60**, 225-248.
- Beaugé C., Ferraz-Mello S., 1993. Resonance trapping in the primordial solar nebula: The case of a Stokes drag dissipation. *Icarus* **103**, 301-318.
- Beaugé C., Ferraz-Mello S., 1994. Capture in exterior mean-motion resonances due to Poynting-Robertson drag. *Icarus* **110**, 239-260.
- Brouwer D., Hori G. I., 1961. Theoretical evaluation of atmospheric drag effects in the motion of an artificial satellite. *Astron. J.* **66**, 193-225.
- Brownlee D. E., 1994. The ring around us. *Nature* **369**, 706.
- Buenzli E., Thalmann C., Vigan A., Boccaletti A., Chauvin G., Augereau J. C., Meyer M. R., Ménard F., Desidera S., Messina S., Henning T., Carson J., Montagnier G., Beuzit J. L., Bonavita M., Eggenberger A., Lagrange A. M., Mesa D., Mouillet D., Quanz S. P., 2010. Dissecting the Moth: Discovery of an off-centered ring in the HD 61005 debris disk with high-resolution imaging. *Astron. Astrophys.* **524**, L1.
- Danby J. M. A., 1988. *Fundamentals of Celestial Mechanics* 2nd edn., Willmann-Bell, Richmond.
- Debes J. H., Weinberger A. J., Kuchner M. J., 2009. Interstellar medium sculpting of the HD 32297 debris disk. *Astrophys. J.* **702**, 318-326.
- Dermott S. F., Jayaraman S., Xu Y. L., Gustafson B. A. S., Liou J.-C., 1994. A circumsolar ring of asteroidal dust in resonant lock with the Earth. *Nature* **369**, 719-723.
- Dermott S. F., Grogan K., Durda D. D., Jayaraman S., Kehoe T. J. J., Kortenkamp S. J., Wyatt M. C., 2001. Orbital evolution of interplanetary dust. In: Grün E., Gustafson B. A. S., Dermott S. F., Fechtig H. (eds.), *Interplanetary Dust*, Springer-Verlag, Berlin, pp. 569-639.
- Dohnanyi J. S., 1978. Particle dynamics. In: McDonnell J. A. M. (ed.), *Cosmic Dust*, Wiley-Interscience, Chichester, pp. 527-605.
- Frisch P. C., Bzowski M., Grün E., Izmodenov V., Krüger H., Linsky J. L., McComas D. J., Möbius E., Redfield S., Schwadron N., Shelton R., Slavin J. D., Wood B. E., 2009. The galactic environment of the Sun: Interstellar material inside and outside of the heliosphere. *Space Sci. Rev.* **146**, 235-273.
- Golimowski D. A., Krist J. E., Stapelfeldt K. R., Chen C. H., Ardila D. R., Bryden G., Clampin M., Ford H. C., Illingworth G. D., Plavchan P., Rieke G. H., Su K. Y. L., 2011. Hubble and Spitzer Space Telescope observations of the debris disk around the nearby K dwarf HD 92945. *Astrophys. J.* **142**, 30.

- Gomes R. S., 1995. The effect of nonconservative forces on resonance lock: Stability and instability. *Icarus* **115**, 47-59.
- Gomes R. S., 1997. Orbital evolution in resonance lock. I. The restricted 3-body problem. *Astron. J.* **114**, 2166-2176.
- Gustafson B. A. S., 1994. Physics of zodiacal dust. *Annu. Rev. Earth Planet. Sci.* **22**, 553-595.
- Hines D. C., Schneider G., Hollenbach D., Mamajek E. E., Hillenbrand L. A., Metchev S. A., Meyer M. R., Carpenter J. M., Moro-Martín A., Silverstone M. D., Kim J. S., Henning T., Bouwman J., Wolf S., 2007. The Moth: An unusual circumstellar structure associated with HD 61005. *Astrophys. J.* **671**, L165-L168.
- Kirkwood D., 1867. *Meteoric Astronomy: A Treatise on Shooting-Stars, Fireballs, and Aerolites* Lippincott J. B. & co., Philadelphia.
- Klačka J., Kómar L., Pástor P., Petržala J., 2008. The non-radial component of the solar wind and motion of dust near mean motion resonances with planets. *Astron. Astrophys.* **489**, 787-793.
- Klačka J., Petržala J., Pástor P., Kómar L., 2012. Solar wind and motion of dust grains. *Mon. Not. R. Astron. Soc.* **421**, 943-959.
- Klačka J., Petržala J., Pástor P., Kómar L., 2014. The Poynting-Robertson effect: A critical perspective. *Icarus* **232**, 249-262.
- Lallement R., Quémerais E., Bertaux J.L., Ferron S., Koutroumpa D., Pellinen R., 2005. Deflection of the interstellar neutral hydrogen flow across the heliospheric interface. *Science* **307**, 1447-1449.
- Leinert C., Grün E., 1990. Interplanetary dust. In: Schwen R., Marsch E. (eds.), *Physics of the Inner Heliosphere I*, Springer-Verlag, Berlin, pp. 207-275.
- Liou J.-C., Zook H. A., 1997. Evolution of interplanetary dust particles in mean motion resonances with planets. *Icarus* **128**, 354-367.
- Maness H. L., Kalas P., Peek K. M. G., Chiang E. I., Scherer K., Fitzgerald M. P., Graham J. R., Hines D. C., Schneider G., Metchev S. A., 2009. Hubble Space Telescope optical imaging of the eroding debris disk HD 61005. *Astrophys. J.* **707**, 1098-1114.
- Margheri A., Ortega R., Rebelo C., 2012. Some analytical results about periodic orbits in the restricted three body problem with dissipation. *Celest. Mech. and Dynam. Astron.* **113**, 279-290.
- Marzari F., 2012. Interstellar medium perturbations on transport-dominated debris discs in binary star systems. *Mon. Not. R. Astron. Soc.* **421**, 3431-3442.



- Marzari F., Thébault P., 2011. On how optical depth tunes the effects of the interstellar medium on debris discs. *Mon. Not. R. Astron. Soc.* **416**, 1890-1899.
- Murray C. D., Dermott S. F., 1999. *Solar System Dynamics* Cambridge University Press, New York.
- Pástor P., 2012a. Influence of fast interstellar gas flow on the dynamics of dust grains. *Celest. Mech. Dyn. Astron.* **112**, 23-45.
- Pástor P., 2012b. Orbital evolution under the action of fast interstellar gas flow with a non-constant drag coefficient. *Mon. Not. R. Astron. Soc.* **426**, 1050-1060.
- Pástor P., 2013. Dust particles in mean motion resonances influenced by an interstellar gas flow. *Mon. Not. R. Astron. Soc.* **431**, 3139-3149.
- Pástor P., Klačka J., Kómar L., 2009. Motion of dust in mean motion resonances with planets. *Celest. Mech. Dyn. Astron.* **103**, 343-364.
- Pástor P., Klačka J., Kómar L., 2011. Orbital evolution under the action of fast interstellar gas flow. *Mon. Not. R. Astron. Soc.* **415**, 2637-2651.
- Pástor P., Klačka J., Petržala J., Kómar L., 2009. Eccentricity evolution in mean motion resonance and non-radial solar wind. *Astron. Astrophys.* **501**, 367-374.
- Poynting J. M., 1904. Radiation in the Solar system: Its effect on temperature and its pressure on small bodies. *Philos. Trans. R. Soc. Lond. Ser. A* **202**, 525-552.
- Reach W. T., Franz B. A., Welland J. L., Hauser M. G., Kelsall T. N., Wright E. L., Rawley G., Stemwedel S. W., Splesman W. J., 1995. Observational confirmation of a circumsolar dust ring by the COBE satellite. *Nature* **374**, 521-523.
- Robertson H. P., 1937. Dynamical effects of radiation in the Solar system. *Mon. Not. R. Astron. Soc.* **97**, 423-438.
- Rodigas T. J., Hinz P. M., Leisenring J., Vaitheeswaran V., Skemer A. J., Skrutskie M., Su K. Y. L., Bailey V., Schneider G., Close L., Mannucci F., Esposito S., Arcidiacono C., Pinna E., Argomedo J., Agapito G., Apai D., Bono G., Boutsia K., Briguglio R., Brusa G., Busoni L., Cresci G., Currie T., Desidera S., Eisner J., Falomo R., Fini L., Follette K., Fontana A., Garnavich P., Gratton R., Green R., Guerra J. C., Hill J. M., Hoffmann W. F., Jones T. J., Krejny M., Kulesa C., Males J., Masciadri E., Mesa D., McCarthy D., Meyer M., Miller D., Nelson M. J., Puglisi A., Quiros-Pacheco F., Riccardi A., Sani E., Stefanini P., Testa V., Wilson J., Woodward C. E., Xompero M., 2012. The gray needle: Large grains in the HD 15115 debris disk from LBT/PISCES/*Ks* and LBTI/LMIRcam/*L'* adaptive optics imaging. *Astrophys. J.* **752**, 57.
- Whipple F. L., 1955. A comet model III. The zodiacal light. *Astrophys. J.* **121**, 750-770.

